Formation of Hydrogels from Plant-based Nanofibers

(Laboratory of Active Bio-based Materials, RISH, Kyoto University)

Kentaro Abe

Social concerns for sustainable green products are encouraging the efficient exploitation of cellulose, the most abundant renewable biopolymer on earth. Because cellulose exists in plant cell walls as highly crystalline nanofibers with several nanometers width, the plant-based cellulose nanofibers display strong mechanical properties and have great potential for reinforcing polymer matrices. Currently the nanofibers can be isolated from various plant sources and we have also found an isolation method in which plant sources are ground in an undried state [1]. The resultant nanofibers had a uniform width of approximately 15nm and a length of more than several micrometers (Figure 1).

Cellulose nanofibers homogeneously dispersed in water without sedimentation and the suspension exhibited a very high viscosity even with 1wt% nanofiber because of the large hydrophilic surface area and entanglement (Figure 2). We focused on the unique properties of nanofiber suspension and found that the novel hydrogels are formed from the cellulose nanofibers by soaking in alkaline aqueous solutions and then neutralization [2]. In general, when making hydrogels from any polymers, they need to be dissolved using suitable solvents. However, because fine cellulose nanofibers behave in water like dissolved polymers, the nanofibers are easily formed into hydrogels while maintaining high crystallinity (Figure 3).

The nanofiber suspensions were converted into two kinds of hydrogels with different crystal forms in response to the increasing concentration of sodium hydroxide (NaOH) and FE-SEM observations demonstrated that both hydrogels formed similar three-dimensional network structures with micro- and nanopores. When treated in 6–9 wt% NaOH, a hydrogel was formed by aggregating the nanofibers with the original morphology and the original crystal form, cellulose I. However, the hydrogel prepared at 15 wt% NaOH had a network formed by the coalescence of cellulose nanofibers and exhibited a highly crystalline cellulose II structure. This gelation process seems to be caused by the axial shrinkage of the cellulose nanofibers in aqueous alkaline solutions.

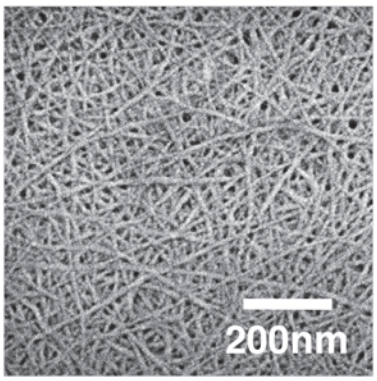

Figure 1. FE-SEM image of cellulose nanofibers isolated from wood

Figure 2. Aqueous suspension of cellulose nanofibers (1 wt%).

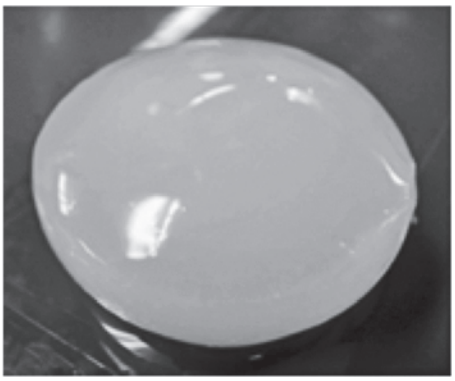

Figure 3. Hydrogel based on the cellulose nanofiber (9wt% NaOH)

References

[1] Abe, K., Iwamoto, S. and Yano, H, "Obtaining cellulose nanofibers with a uniform width of 15 nm from wood", *Biomacromolecules*, vol. 8, no. 10, pp. 3276-3278, 2007.

[2] Abe, K. and Yano, H, "Formation of hydrogels from cellulose nanofibers", *Carbohydrate Polymers*, vol. 85, no. 4, pp. 733-737, 2011.

Middle atmospheric chemistry and dynamics: results from the Superconducting Submillimeter-Wave Limb-Emission Sounder (SMILES)

(Laboratory of Atmospheric Environmental Information Analysis, RISH, Kyoto University)

Masato Shiotani

The Superconducting Submillimeter-Wave Limb-Emission Sounder (SMILES) was developed to be aboard the Japanese Experiment Module (JEM) on the International Space Station. SMILES was successfully launched by the H-IIB rocket with the H-II Transfer Vehicle on September 11, 2009, was attached to JEM on September 25, and started atmospheric observations on October 12. Unfortunately, SMILES observations have been suspended since April 21, 2010 due to the failure of a critical component in the submillimeter local oscillator. However, high-sensitivity measurements of minor species had been performed by a receiver using superconductor- insulator- superconductor (SIS) mixers, cooled to 4.5 K by a compact mechanical cryocooler. Thus global and vertical distributions of about ten atmospheric minor constituents related to the ozone chemistry are derived. The mission objectives are as follows: i) To demonstrate a 4-K mechanical cooler and superconducting mixers in the environment of outer space for submillimeter limb-emission sounding and ii) To measure atmospheric minor constituents in the middle atmosphere globally in order to gain a better understanding of factors and processes controlling the stratospheric ozone amounts and those related to climate change. Since the ISS has a circular orbit with an inclination angle of 51.6 degrees, no observations in the polar latitude are available. To measure northern high-latitude regions the antenna beam is tilted 45 degrees left from the direction of orbital motion, enabling SMILES to observe latitudes from 38°S to 65°N. Another important aspect of the SMILES observation is that SMILES can measure the atmosphere at different local times because of the non-sun-synchronous ISS orbit. Measurements of diurnal variation of the atmospheric minor species are expected to provide further insights into the atmospheric science. The SMILES measurements have been processed to provide unique observational results in association with middle atmospheric chemistry and dynamics, thus these results demonstrate SMILES abilities to observe the atmospheric minor constituents in the middle atmosphere.

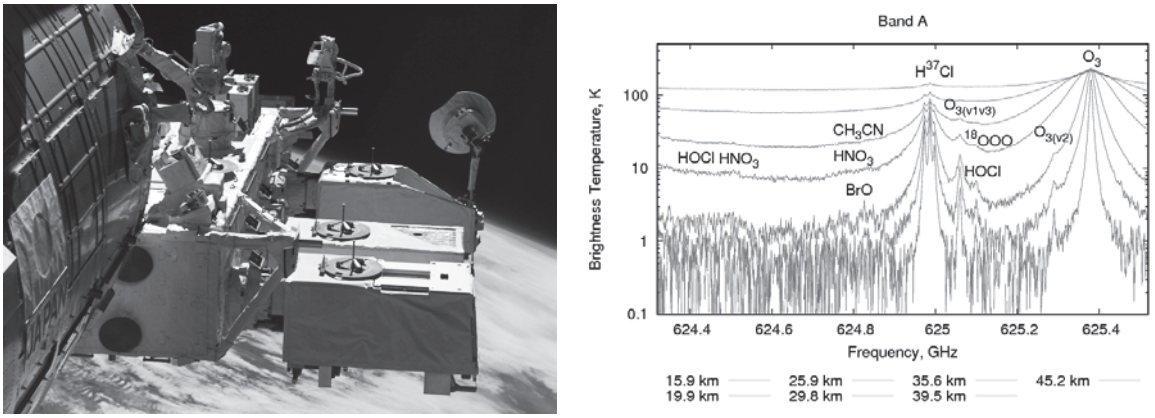

Figure 1. (left) The SMILES instrument (second from the front) attached to the Japanese Exposed Facility on the International Space Station. (right) Observed spectra at several altitudes for Band A measured at 03:22:14 UT on October 12, 2009 at 23.30°N and 173.83°E.

References

[1] Kikuchi, K., *et al.*, "Overview and early results of the Superconducting Submillimeter-Wave Limb-Emission Sounder (SMILES)," *J. Geophys. Res.*, 115, D23306, doi:10.1029/2010JD014379, 2010.

Application of Microwave Power Transmission

(Laboratory of Applied Radio Engineering for Humanosphere, RISH, Kyoto University)

Naoki Shinohara and Tomohiko Mitani

In our laboratory, there are three main research topics as follows;

- Research of Space Solar Power Station/Satellite (SPS)
- Research of Microwave Power Transmission (MPT) for Various Applications
- Research of Advanced Microwave Processing for Biomass Refinery and Creation of New Materials

In FY2010, we started inter-university collaborative research with a new anechoic chamber with clean room and high power microwave absorbers and high efficiently new phased array with GaN amplifiers and MMIC phase shifters for the SPS and MPT.

Research Activities for the SPS

Based on the inter-university collaborative research, we developed some new MPT system. For the SPS, it is necessary to properly deal with the heat which is generated from power amplifier. We studied the antenna structure which conducted heat form power amplifier to antenna and radiated heat from the antenna surface with IHI Aerospace co., ltd. Via holes in the antenna can conduct heat from the back surface of antenna to the surface of one. The antenna is a crossed slot antenna, which can radiate heat efficiently because the metal surface is large. The antenna has a wavelength selection sheet on the antenna to cut heat from outside to the antenna and radiate heat efficiently. In this paper, we report the results of the thermal characterization test of the antenna.

Collaborative Researches of the MPT applications

We designed and fabricated the rectennas which use class-F load as an output filter in order to develop highly efficient rectennas at 24GHz and 60GHz with NTT co. We also fabricated conventional rectennas which use a capacitor as an output filter, and compared the efficiency of class-F load rectennas with that of capacitor rectennas. We selected the diode which can produce high efficiency even at high frequency, and we parallelized the diode to improve the efficiency. The experimental result of efficiency of class-F load rectennas was 65.6%, on the other hand, that of capacitor rectennas was 52.1%.

Microwave Pretreatment System for Bioethanol Production from Woody Biomass

Efficient pretreatment prior to enzymatic saccharification process is essential for profitable bioethanol production from woody biomass. Microwave pretreatment is expected as an efficient and energy-cost-saving method to enhance enzymatic susceptibility. The objective of the present study is to develop an efficient, high-volume, and continuous microwave pretreatment system toward commercially-based bioethanol production. As a feasibility study, we developed prototypes of a continuous-flow-type microwave pretreatment system for bioethanol production from woody biomass. A unit of the microwave irradiation sections of a continuous-flow-type microwave pretreatment system was designed with a 3D electromagnetic simulator. Prototype experiments and quantitative estimation of energy balance were also conducted. Microwave pretreatment provided 45.9% of the total saccharide yield woody biomass weight by electric consumption of 552 kJ; whereas conventional heating pretreatment provides 43.6 % of the total saccharide yield by 498 kJ, when the mixture was composed of 70 g of woody biomass (Japanese cedar sapwood chips) and 770 g of solvents (ethylene glycol : phosphoric acid = 95 : 5). We estimated 14.8g of bioethanol and 439 kJ of bioethanol energy could be produced by the prototype microwave pretreatment. Although heat dissipation from the metal pipe to the air and the ratio of solvents to woody biomass are immediate problems, microwave is a future potential energy-saving pretreatment method without loss of the saccharide yield.

UV Raman lidar for profiling atmospheric water vapor

(Laboratory of Atmospheric Sensing and Diagnosis, RISH, Kyoto University)

Masanori Yabuki, Chikara Miyawaki, and Toshitaka Tsuda

Measurements of the atmospheric water vapor over all timescales and extensive spatial regions are essential for studies of air quality, local weather, and climate change. The Raman lidar is a laser-based remote sensing instrument that is used for profiling the water vapor mixing ratio, the atmospheric temperature, and several cloud- and aerosol-related quantities. Raman lidar applications are based on the measurements of the weak inelastic scattering of light by molecules with frequency shift characteristics, as a function of the range. Since 2000, we have developed several Raman lidar systems for measuring water vapor. One such system is the lidar installed at Shigaraki MU Radar Observatory, Japan; it is designed for high-sensitivity water vapor measurements at an altitude range of 1.5–10 km with a high-power laser and a large telescope. Other systems include the portable Raman lidar that can be transported using a one-box-type vehicle and used for studying the distribution of the water vapor in the lower troposphere in various observation fields such as volcanoes and forests. These Raman lidar systems use a visible laser wavelength because of the quality limitations of optical components such as narrow-band interference filters, although the visible laser wavelength is not always safe for human eyes.

In atmospheric measurements using a laser-based system, the prevention of damage to human eyes caused by the transmitted laser radiation is an important issue. With regard to eye safety, the UV laser has an advantage over the wavelengths in the visible because the maximum permitted exposure is larger by 3–4 orders of magnitude in the UV region than in the visible region. Recently, the improved performance of UV optical components has led to the development of better UV Raman lidar systems; the system is as highly sensitive and cost effective as the visible system. Additionally, UV lidars may achieve better daytime performances than visible systems because of the reduced sky background. Hence, we have developed a water vapor Raman lidar using a UV laser. This UV Raman lidar is equipped with a 25-cm receiving telescope at a Nd:YAG laser wavelength of 354.7 nm and is used for measuring the light separated into an elastic backscatter signal and vibrational Raman signals of nitrogen and water vapor at wavelengths of 354.7, 386.8, and 408.0 nm, respectively. An example of the water vapor mixing ratio profile obtained using the developed UV Raman lidar and a radiosonde at nighttime at Uji, Kyoto, is depicted in Fig. 1. The trends shown by the lidar and the radiosonde agree well up to 7 km for a height and time resolution of 108 m and 30 min, respectively. This UV Raman lidar is suitable for measuring the atmospheric water vapor in highly populated areas and near the earth's surface. The fact that the UV lidar poses less danger to the human eye may make it favorable for use as a scanning system. This UV system has been used for continuous water vapor measurements in the urban area for validating the ground-based GPS (GNSS) meteorological observations. Moreover, we plan to use the UV lidar for simultaneous measurements with tethered balloon profiling for trace gases and aerosols in order to elucidate the properties of the minor atmospheric constituents of the earth's surface layer.

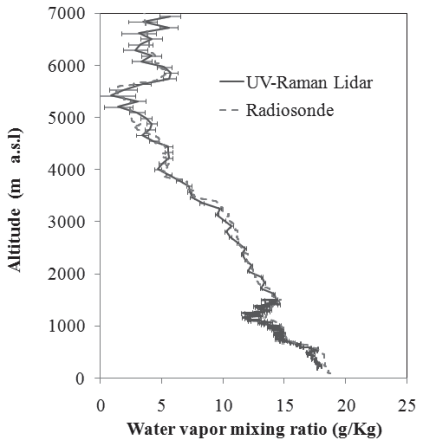

Figure 1. Water vapor mixing ratio profiles from the UV Raman lidar and the radiosonde at Uji, Kyoto, at 00:00–00:30 JST on July 9, 2011. Height resolution is 11 m for 200–1500 m and 108 m for 1500–7000 m. Error bars show the statistical uncertainty due to signal noise. The radiosonde was started at 00:00 JST.

Acknowledgements

This work is supported in part by the Grant-in-Aid for Promoting Space Utilization of the Ministry of Education, Culture,Science and Technology (MEXT).

Bioethanol production from woody biomass using microwave technology

([1]Laboratory of Biomass Conversion, [2]Laboratory of Applied Radio Engineering for Humanosphere, RISH, Kyoto University)

Takashi Watanabe[1], Tomohiko Mitani[2] and Naoki Shinohara[2]

There is growing demand to develop new, highly efficient technology to produce bioethanol and chemicals from woody biomass. For enzymatic conversion of lignocellulosics, pretreatments to expose cell wall polysaccharides is necessary. Efficient conversion of the enzymatic hydrolyzates by ethanologenic microbes are also the key factor for bioethanol production. In our NEDO project (R&D member: RISH, Kyoto Univ., Prof. Hideshi Yanase, Fac. Eng. Tottori Univ., Japan Chemical Engineering & Machinery Co. Ltd., and Toyota Motor Corporation), we have applied microwave-assisted solvolysis to the pretreatment. We have developed microwave solvolysis system with various catalysts and new continuous microwave reactors by applying 3D electromagnetic simulation technique[1-6]. Through cell-surface engineering based on genome DNA analysis, novel, high-performance ethanologenic bacteria, *Zymobacter palmae* and *Zymomonas mobilis,* which efficiently convert hexoses and pentoses to bioethanol, secrete β-glucosidase, and display cellulase on the surface of the cells, are being bred in Tottori Univ. A high-performance fermentation process using the ethanologenic bacteria is being developed to produce bioethanol from fast growing wood. A bench scale plant for bioethanol production using the pretreatment system and genetically engineered bacteria was build in 2010 (Fig. 1), and bioethanol was produced in a 300 L-scale jar fermentor. Production of value-added aromatic chemicals from lignin is indispensable to replace oil refinery to biorefinery. Therefore, we have been studying conversion of lignin to functional polymers and low molecular mass aromatics by microwave reactions. We also investigate detailed structures of pretreated lignocellulosics and their components by ultra-high sensitivity NMR, ultra-high resolution mass spectroscopy and fluorescent-labeled carbohydrate binding modules (CBM), aiming at maximizing conversion efficiency with minimum enzyme dosage and energy[7,8].

Fig. 1 Bench scale plant for bioethanol production from woody biomass (NEDO project).

Acknowledgements

The authors gratefully acknowledge our collaborators from the two laboratories in RISH, Prof. Hideshi Yanase, Tottori Univ., Japan Chemical Engineering & Machinery Co. Ltd., and Toyota Motor Corporation.

References

[1] Sasaki, C. et al., *Biores. Technol.*, in press (2011).
[2] Verma, P. et al., *Biores. Technol.*, **102**, 3941-3945 (2011).
[3] Baba, Y. et al., *Biomass & Bioenergy*, **35**, 320-324 (2011).
[4] Liu, J., R. et al., *Biores. Technol*., **101**, 9355-9360 (2010).
[5] Mitani, T. et al., *J. Japan Inst. Energy*, in press (2011).
[6] Watanabe, T., T. Mitani, Microwave Technology for Lignocellulosic Biorefinery, "The Role of Green Chemistry in Biomass Processing and Conversion", eds. by H. Xie and N. Gathergood, John Wiley & Sons, New Jersey, in press (2011).
[7] Kawakubo, T. et al., *Biotechnol. Bioeng.*, **105**, 499-508 (2010).
[8] Yoshioka, K. et al., *Phytochem. Anal*., in press (2011).

Xylarium database and its network

(Laboratory of Biomass Morphogenesis and Information, RISH, Kyoto University)

Junji Sugiyama

Inter-university network on wood diversity

Wood collections are indeed important historical as well as academic records not only in wood science, but rather broad area including chronology, climatology, archeology, history, and so on. Therefore, by making use of the cooperative research function equipped in our institute, the attempts to unify wood database, with participation of Hokkaido University, Tohoku University, the University of Tokyo, Forest and Forest Product Research Institute, Kyoto University and Kyushu University, has been started, and first preliminary results came out. This year, for instance, SEM digital image database from "Ohtani Collection" in Hokkaido University(Fig. 1), digital list of Tohoku University's fossil wood collections, became in good order, and furthermore, regeneration of deteriorated preparation for optical microscopy in Kyushu University have been started.

As for our xylarium database, detailed descriptions and digital data on old wood collections from historical buildings are added. The data includes, dimension, density, high-resolution scan on the transverse face, color, age, usage, and geographic information of the corresponding buildings or artefacts, from nearly 400 specimens.

In addition, in order to visualize our activity better (mi-e-ru-ka), digital archives for visitors were newly prepared and the contents are available by mobile multimedia devices equipped in the virtual field.

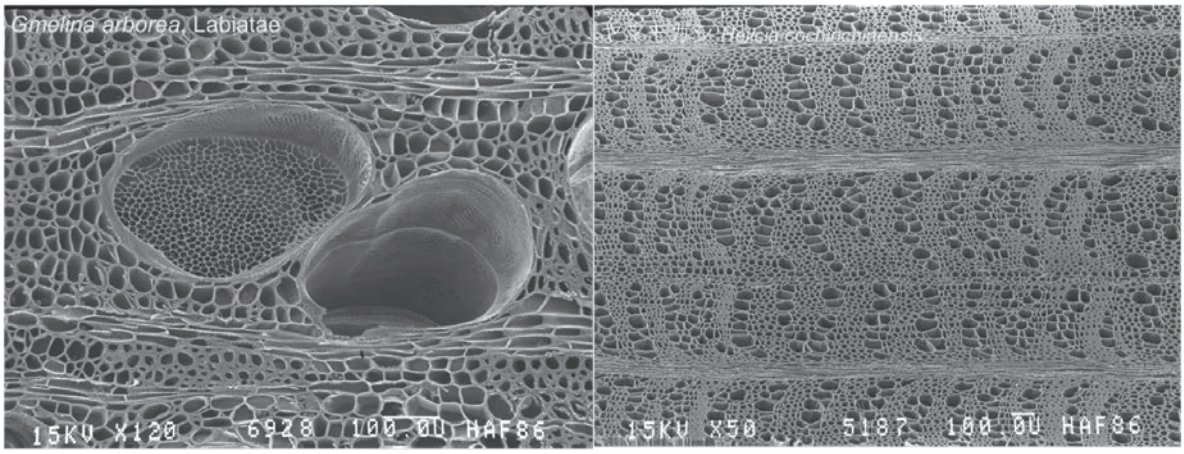

Figure 1 An example of SEM micrographs from "Ohtani collection" (Hokkaido University Database) . Courtesy of Dr. Yuzo Sano.

Acknowledgements

The project was supported by Grant-in-Aid for Publication of Scientific Research Results (database) from The Ministry of Education, Culture, Sports, Science and Technology (MEXT) as well as RISH cooperative research project (Humanosphere database).

Simulation Studies on Formation of Earth's Radiation Belt and Ring Current

(Laboratory of Computer Simulation for Humanospheric Sciences, RISH, Kyoto University)

Yoshiharu Omura, and Yusuke Ebihara

Theory and observation of electromagnetic ion cyclotron triggered emissions

Electromagnetic ion cyclotron (EMIC) waves are suggested to play a significant role in the dynamics of the Earth's radiation belt and the ring current. We develop a nonlinear wave growth theory of EMIC triggered emissions observed in the Earth's magnetosphere. After deriving the basic wave equations from Maxwell's equations and the momentum equations for the electrons and ions, we obtain equations that describe the nonlinear dynamics of resonant protons interacting with an EMIC wave. The frequency sweep rate of the wave plays an important role in forming the resonant current that controls the wave growth. Assuming an optimum condition for the maximum growth rate as an absolute instability at the magnetic equator and a self-sustaining growth condition for the wave propagating from the magnetic equator, we obtain a set of ordinary differential equations that describe the nonlinear evolution of a rising tone emission generated at the magnetic equator. Using the physical parameters inferred from observations by the Cluster spacecraft, we determine the dispersion relation for the EMIC waves. Assuming saturation of the wave amplitude, as is found in the observations, we find good agreement between the numerical solutions and the wave spectrum of the EMIC triggered emissions. [1]

Microburst precipitation of energetic electrons

Energetic electrons are often observed to precipitate into the Earth's atmosphere with a short duration (<1 sec). This is called an electron microburst, which comprises an important loss process from the outer radiation belt. By means of a self‐consistent full‐particle simulation, we show that microburst precipitation of electrons with energies ranging between 10 keV and 100 keV accompanies the generation of discrete bursty chorus wave emissions. We demonstrate a one‐to‐one correspondence between the electron microbursts and the generation of discrete chorus elements. This simulation study is the first to establish such an exact correlation between electron microbursts and the generation of chorus elements. [2]

Rapid recovery of storm-time ring current

The Earth's ring current sometimes exhibits rapid decay, but the underlying mechanism was unknown. We perform a simulation of energetic ions that constitute the ring current. When we include the field line curvature (FLC) scattering of the ions, the ring current shows rapid recovery with an e-folding time of ~6 h, which is consistent with observations. However, without FLC scattering, the ring current shows a slower recovery with an e-folding time of ~12 h. Energetic neutral hydrogen with energy ≥ 39 keV is significantly reduced by the FLC scattering, which is consistent with data from the IMAGE satellite. Power of precipitating protons also shows a fairly good agreement with data from IMAGE. We conclude that the FLC scattering is a significant loss mechanism for the ring current. [3]

References

[1] Y. Omura, J. Pickett, B, Grison, O. Santolik, I. Dandouras, M. Engebretson, P. M. E. Décréau, and A. Masson, "Theory and observation of electromagnetic ion cyclotron triggeredemissions in the magnetosphere", *Journal of Geophysical Research*, 115, A07234, doi:10.1029/2010JA015300, 2010.

[2] M. Hikishima, Y. Omura, and D. Summers, "Microburst precipitation of energetic electrons associated with chorus wave generation", *Geophysical Research Letters*, 37, L07103, doi:10.1029/2010GL042678, 2010.

[3] Y. Ebihara, M. –C. Fok, T. J. Immel, and P. C. Brandt, "Rapid decay of storm time ring current due to pitch angle scattering in curved field line", *Journal of Geophysical Research*, 116, A03218, doi:10.1029/2010JA016000, 2011.

Laboratory method to determine termite-resistance of plastics

(Laboratory of Innovative Humano-Habitability, RISH, Kyoto University)

Kunio Tsunoda

There is no standardized methodology worldwide to assess the resistance of plastic materials to subterranean termites in both the laboratory and the field. However, the development of new plastic materials always necessitates the reliable comparison between new and existing products. Early studies by Gay and Wetherly [1, 2] and Watson [3] indicated that laboratory evaluations with Australian termite species were effective for comparing the resistance of various plastics to termites and could reproduce the termite-susceptibility of plastics in the field test by others [4,5]. However, they were forced to sacrifice the relatively large quantity of termites. A new method in which plastic samples were exposed to a nest of *Coptotermes formosanus* Shiraki was proposed and proved applicable to the evaluation of comparative termite-resistance [6]. Existing Japanese standardized laboratory methods were proved to be unsuitable for evaluating the termite-resistance of plastics in any form [7,8]. One of the modified Japanese standardized methods that were applicable to evaluating termite-resistance of plastics would not sacrifice many termites, and it was possible to standardize the method to compare the termite-resistance of non-woody materials with or without chemical treatment as shown in Figs. 1 and 2. The termite density of 24 workers/cm^2 foraging area was high enough for *C. formosanus* to cause visible attack on straight face [6].

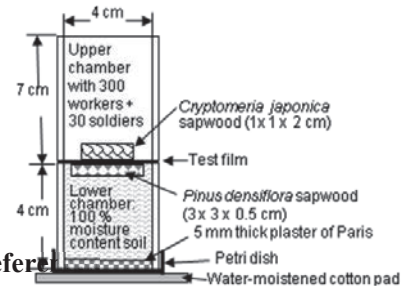

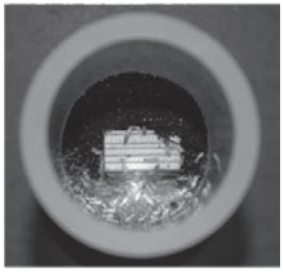

Fig. 1 (left) Experimental device composed of two acrylic cylinders
Fig. 2 (right) Termite penetration through a susceptible HDPE film: penetration took place within 2-3 days after the initiation of test; soil on the film surface is the sign of termite penetration

Refere

[1] Gay, F. J, and A. H. Wetherly Laboratory studies of termite resistance. IV. The termite resistance of plastics. Division of Entomology (CSIRO, Melbourne, Australia) Technical. Paper No. 5, 31 pp. 1962
[2] Gay, F. J, and A. H.Wetherly. Laboratory studies of termite resistance. V. The termite resistance of plastics. Division of Entomology (CSIRO, Melbourne, Australia) Technical. Paper No. 10, 49 pp. 1969
[3] Watson, J. A. L., Z. R.Dai and R. A.Barrett. Comparative studies on the resistance of materials to species of *Coptotermes* (Isoptera: Rhinotermitidae). I. The susceptibilities of various plastics to *C. acinaciformis* (Froggatt) from Australia and *C. formosanus S*hiraki from China. *Bulletin of Entomological Research* 74, 495-503. 1984
[4] Beal, R. H., J. D. Bultman and C. R. Southwell Resistance of polymeric cable coverings to subterranean termite attack. *International Biodeterioration Bulletin 9, 28-34. 1973*
[5] Beal, R. H. and J. D. Bultman Resistance of polymeric cable coverings to subterranean termite attack after eight years of field testing in the tropics. *International Biodeterioration Bulletin* 14, 123-127. 1978
[6] Tsunoda, K., G. Rosenblat and K. Dohi Laboratory evaluation of the resistance of plastics to subterranean termite *Coptotermes formosanus* (Blattodea: Rrhinotermitidae). *International Biodeterioration & Biodegradation* 64, 232-237.2010
[7] Rosenblat, G., w. j. Hwang and K. Tsunoda Laboratory evaluation of the termite resistance of polyamide. *Proceedings of the 2nd Conference of the Pacific Rim Termite Research Group* (February 28-March 1, 2005, Bangkok, Thailand), 61-64. 2005
[8] Rosenblat, G. and K. Tsunoda Laboratory evaluation of the termite resistance of plastic tubes. *Proceedings of the 3rd Conference of the Pacific Rim Termite Research Group* (March 6-7 2006, Guangzhou, P. R. China), 89-90.2006

Development of high-throughput lignin determination and characterization methods and discovery of oxalate transporter from *Fomitopsis palustris*

(Laboratory of Metabolic Science of Forest Plants and Microorganisms, RISH, Kyoto University)

Toshiaki Umezawa, Takefumi Hattori, and Shiro Suzuki

It is becoming more important to establish a sustainable society, which depends on renewable resources. Wood biomass is the most abundant renewable resource on the earth, and therefore, the better utilization and efficient production of wood biomass are the key factors to establish a sustainable society. In this context, our laboratory is involved in analyzing metabolic functions of forest plants and microorganisms from a wide variety of aspects, including organic chemistry, biochemistry, molecular biology, and metabolomics, aiming at the elucidation of mechanisms of wood formation of biomass plants, degradation of wood by wood-rotting fungi, and symbiosis of ectomycorrhizal fungi with forest trees, and their biotechnological application. Here we describe the recent research topics of our laboratory.

1. Development of high-throughput lignin determination and characterization methods

In molecular breeding of wood biomass plants, straight-forward, high-throughput, and microscale characterization of wood biomass components is important to select the best recombinant lines at the stage of juvenile plantlets. Because lignin is one of the major components in wood biomass, its biosynthesis is one of the major targets in molecular breeding of wood biomass plants. However, the conventional methods for lignin analysis are low-throughput and employ complicate experimental steps. Recently we modified the thioglycolic acid lignin determination and nitrobenzene oxidation method suitable for large number and small quantity of samples [1-3]. Using the analytical methods, we are selecting the rice plants to enable the efficient conversion of wood biomass to energy.

2. Discovery of oxalate transporter from *Fomitopsis palustris*

An oxalate-fermenting brown-rot fungus, *Fomitopsis palustris*, secretes large amounts of oxalic acid during wood decay. The acid is indispensable for the degradation of wood cell walls. We isolated a cDNA, *FpOAR* (*Fomitopsis palustris* Oxalic Acid Resistance), from *F. palustris* by functional screening of yeast transformants with cDNAs grown on oxalic acid-containing plates. The yeast transformant possessing *FpOAR* (*FpOAR*-transformant) acquired resistance to oxalic acid and contained less oxalate than the control transformant with an empty vector. Biochemical analyses using membrane vesicles of the *FpOAR*-transformant showed the oxalate transport property of FpOAR. FpOAR is strongly suggested to play an important role in wood decay by acting as a secondary transporter responsible for secretion of oxalate by *F. palustris* [4].

References

[1] S. Suzuki, Y. Suzuki, N. Yamamoto, T. Hattori, M. Sakamoto, T. Umezawa, "High-throughput determination of thioglycolic acid lignin from rice," *Plant Biotechnology*, vol. 26, pp. 337-340, 2009.

[2] M. Yamamura, T. Hattori, S. Suzuki, D. Shibata, T. Umezawa, "Microscale alkaline nitrobenzene oxidation method for high-throughput determination of aromatic components," *Plant Biotechnology*, vol. 27, pp. 305-310, 2010.

[3] M. Yamamura, S. Wada, N. Sakakibara, T. Nakatsubo, S. Suzuki, T. Hattori, M. Takeda, N. Sakurai, H. Suzuki, D. Shibata, T. Umezawa, "Occurrence of guaiacyl/p-hydroxyphenyl lignin in *Arabidopsis thaliana* T87 cells," *Plant Biotechnology*, vol. 28, pp. 1-8, 2011.

[4] T. Watanabe, N. Shitan, S. Suzuki, T. Umezawa, M. Shimada, K. Yazaki, T. Hattori, "Oxalate efflux transporter from the brown-rot fungus *Fomitopsis palustris*, "*Applied and Environmental Microbiology*, vol. 76, pp. 7683-7690, 2010.

Involvement of Auxin Distribution on the Nodule Development in a model legume plant, *Lotus japonicus*

(Laboratory of Plant Gene Expression, RISH, Kyoto University)

Kojiro Takanashi, Akifumi Sugiyama and Kazufumi Yazaki

Legume plants establish symbiosis with rhizobia in soils by forming organ called nodules, where symbiotic nitrogen fixation occurs. The initiation of nodule formation by rhizobia is stimulated by a signaling molecule from rhizobia, Nod factor, and nodules are mostly developed from outer cortical cells and form spherical nodules in determinate legumes as *Lotus japonicus*. This nodule formation process is regulated by several phytohormones, such as auxin, cytokinins, gibberellins, and brassinosteroids as positive regulators of nodule formation, while ethylene, jasmonic acid and abscic acid as negative regulators. Auxin regulates plant growth and development, particularly by the regulated polar movement along the vertical axis, forming concentration gradient through-out the plant. Inhibitors of auxin transport such as 1-naphtylphthalamic acid (NPA) and tri-indobenzoic acid (TIBA) have been generally employed to observe the effect of the auxin transport. Another biochemical tool to study auxin functions is α-(phenyl ethyl-2-one)-indole-3-acetic acid (PEO-IAA) as an auxin antagonist. We have investigated the auxin distribution in the determinate nodules of *L. japonicus* using auxin inhibitors and found that the development of lenticels and nodule vascular bundles were was strongly affected by auxin during the nodulation process.

The auxin responsible GH3:GUS transformant of *L. japonicus* showed auxin responses in a nodulation-specific manner during nodule development. Before inoculation of *Mezorhizobium loti*, GH3 expression was observed only in central cylinder, while after inoculation, GH3 expression started to increase in cortical cells in nodule primordial where cell divisions occur. In mature nodules, GUS staining disappeared, whereas strong expression was observed in vascular tissues. These results suggest that an important role of auxin in nodule formation, especially in the development of vascular tissues. By using auxin inhibitors, we have demonstrated the effects of auxin transport inhibitors on nodulation by showing that the treatment of *L. japonicus* with NPA or TIBA altered the nodule number at concentrations 10 μM and 100 μM. We also investigated the effects of PEO-IAA on nodulation in *L. japonicus*. Although PEO-IAA affected the root growth and root hair formation in *L. japonicus*, the number of nodules was not strongly altered. The effect of PEO-IAA was observed in the development of lenticels on nodules. We also found the inhibition of the development of nodule vascular bundle by these inhibitors.

Lenticels, which develop opposite the nodule vascular bundle, are suggested to arise from specific phellogen cells in the nodule cortex. Lenticels appear on the nodule surface, and they regulate gas permeability of nodules. The relation between the lenticels and the nodule vascular system is not yet known; however, it was suggested that the development of lenticel is associated with growth substances supplied from the vascular system, suggesting that auxin is necessary to form nodule vascular bundle and lack of lenticel is an indirect effect of the inhibition, or auxin is a growth substance of lenticels.

We have shown the involvement of auxin in formation of nodule vascular bundle and lenticel. For further understanding of the auxin distribution and the role of auxin in the nodule formation of *L. japonicus*, we need to identify and characterize auxin transporters involved in the nodulation

Acknowledgements

We would like to thank Dr. Ken-ichiro Hayashi (Okayama University of Science, Japan) for the PEO-IAA, and Dr. Niels Sandal and Dr. Jens Stougaard (University of Aarhus, Denmark) and Dr. Herman P. Spaink (Leiden State University, Netherlands) for seeds of GH3:GUS transformants.

References

[1] Takanashi K, Sugiyama A, Yazaki K, "Involvement of auxin distribution in root nodule development of *Lotus japonicus*", *Planta*, vol. 234, no. 1. pp. 73-81, 2011.

Portable X-band Doppler weather radar as a new tool for disaster prevention and water resource monitoring

(Laboratory of Radar Atmospheric Science, RISH, Kyoto University)

Masayuki K. Yamamoto, Hiroyuki Hashiguchi, and Mamoru Yamamoto

A portable X-band Doppler weather radar (XDR), which can be carried by a cart and hence can be installed at very small areas such as rooftop area of small building, has been developed. XDR is composed of the outdoor and indoor units. Components of the outdoor unit (a parabolic antenna with a diameter of 1.2 m, magnetron transmitter, and radio frequency (RF) and intermediate frequency (IF) analog components) are housed in a compact body with a weight less than 300 kg. The radar operation, IF digital processing, and data storage are carried out by a desktop computer in which a commercial IF digital receiver is installed. Using the dataset collected from 25 to 26 October 2009 at the Shigaraki MU Observatory (34°51N, 136°06'E), Japan, equivalent radar reflectivity factor (Z_e) and Doppler velocity (V_d) measured by XDR were assessed using a Micro Rain Radar and a L-band Doppler radar named LQ-7. The assessment results using correlation coefficients and regression lines demonstrate that XDR measured Z_e and V_d accurately.

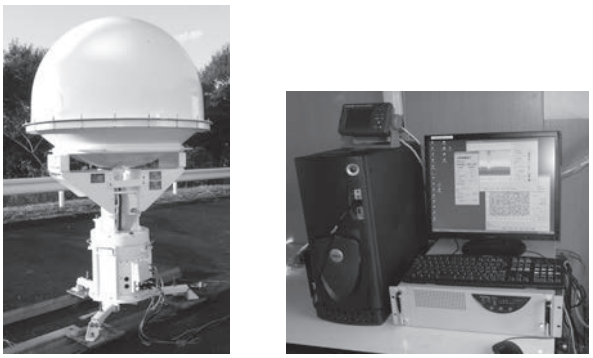

Figure. Outside view of (left) the outdoor and (right) indoor unit of the XDR.

Acknowledgements

XDR were designed by Mitsubishi Electric TOKKI Systems Corporation, and their development were supported by the Meteorological Research Institute (MRI), Japan Meteorological Agency (JMA) under the program of Special Coordination Funds for Promoting Science and Technology named "Japanese Cloud Seeding Experiments for Precipitation Augmentation (JCSEPA)." JCSEPA program is funded by the Ministry of Education, Culture, Sports, Science and Technology of Japan (MEXT).

References

[1] Yamamoto M. K., et al., Doppler velocity measurement of portable X-band weather radar equipped with magnetron transmitter and IF digital receiver, *IEICE Trans. Commun.*, **E94-B(6)**, 1716-1724, doi:10.1587/transcom.E94.B.1716, 2011.

[2] Ikeno, N., Assessment of radar reflectivity factor and Doppler velocity measured by portable X-band and Ka-band Doppler weather radars, this issue.

Collaborative Research on Static as well as Dynamic Performance of Taiwanese Traditional Timber Frame Structures

(Laboratory of Structural Function, RISH, Kyoto University)

Kohei Komatsu, Takuro Mori and Akihisa Kitamori

On the end of March in 2010, a MOU between College of Planning and Design, National Cheng Kung University (NCKU), Taiwan and RISH, Kyoto University, Japan was concluded. As a symbolic gift from NCKU for this MOU conclusion, two types of Taiwanese traditional wooden frame specimens were presented due to the courtesy of Professor Min-fu Hsu who is a key person for this MOU and has stayed in RISH for three months as an invited professor. On accepting these precious presents, we conducted static push-pull cyclic lateral mixed with constant vertical loading test on these traditional partial full-scale timber frame specimens and also did a shaking table test on Taiwanese Kumimono-complex to make the mechanical behaviors of Taiwanese traditional timber structure more clear. Figure 1 shows the test set-up of Taiwanese traditional timber frame specimen made of Taiwanese Hinoki which was originally collected from part of the "Doorway Hall" of the "Ancestral Hall" for Chung Family at Ping-tung County in South of Taiwan. In addition to this, one more replica specimen made of Taiwanese Cedar was newly built and tested. Figure 2 indicates load-deflection relationship of these two specimens. From these hysteresis loops, it is clear that they behaved in the same manner as Japanese traditional frame structure in which the effect of "thick column-restoring force" took important roles.

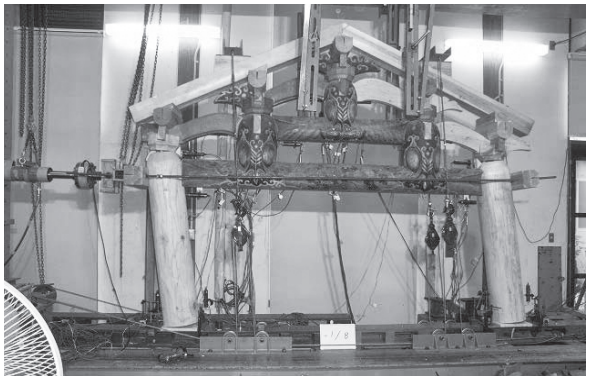

Fig.1 Test set-up of Taiwanese frame specimen.

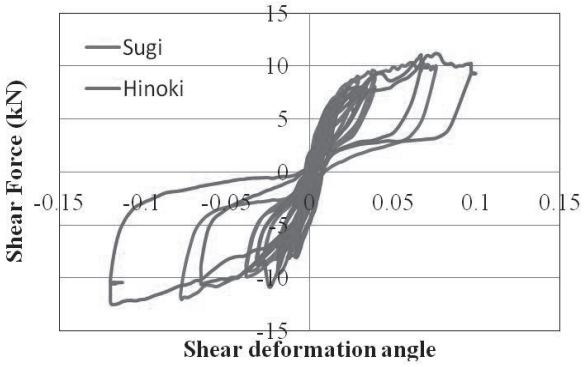

Fig.2 Load-deflection relationships.

Figure 3 shows a shaking table test on a Kumimono-complex taken from another Taiwanese traditional timber structure in Taiwan and was transported from NCKU for our collaboration research activity. This dynamic test was conducted at Chubu University as a part of another collaborative research of three institutes, namely RISH, NCKU and Chubu University.

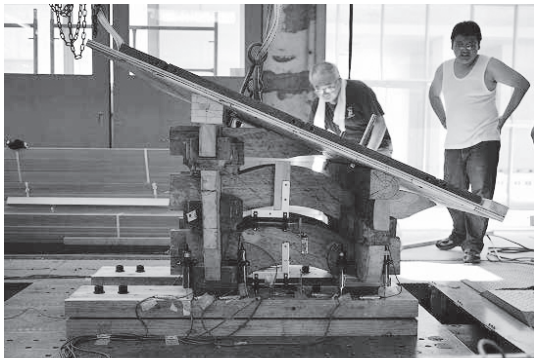

Fig.3 A partial full-scale Kumimono-complex specimen put on the shaking table equipment.

Acknowledgment :

All experimental and analytical works on this collaborative research were conducted with Dr. Wen-Shao Chang, who was a visiting research scientist from Taiwan, having a financial support from JSPS foreign scientist budget. While the shaking table test was done by using facility at Chubu University under the supervision of Professor Y. Kataoka and Assistant Professor T.Wakita. Authors would like to express their sincere thanks to all of them.

Curing and degradation processes of cement-bonded particleboard by supercritical CO_2 treatment

(Laboratory of Sustainable Materials, RISH, Kyoto University)

Rohny Setiawan Maail, Kenji Umemura, Hideo Aizawa, Shuichi Kawai

Cement-bonded particleboard (CBP) and its application in the building industry have been rapidly accepted in many countries because of its excellent exterior properties. In the development of CBP, many studies have focused on understanding the utilization of carbon dioxide (CO_2) in the manufacturing process. Using of gaseous or supercritical CO_2 accelerated the curing process rapidly and enhanced the mechanical properties of board [1]. On the other hand, it has often been reported that CO_2 degrades the cement or concrete because of carbonation, however, it has not yet been revealed whether the supercritical CO_2 treatment has a positive or negative effect on the performance of CBP over a longer time span. We aim to clarify the curing and degradation processes of CBP under the supercritical CO_2 treatment.

We have manufactured CBP using Japanese cypress (*Chamaecyparis obtusa* Endl) and Japanese cedar (*Cryptomeria japonica* D.Don) with a target density of 1.2 g/cm^3 at a cement/wood particle/water weight ratio of 2.5:1.0:1.25. As references, we have manufactured neat cement board (NC) and $Ca(OH)_2$ board. Hand-formed mat of 230 x 230 mm was cold-pressed to a targeted thickness of 12 mm and kept in an oven set at 60^{o}C for 24 h. Four specimens of 50 x 210 mm prepared from these boards were then used for curing treatment. The three curing treatments were (1) supercritical CO_2 treatments, 10 min to 10 days; (2) conventional curing treatment for 28 days (Conventional); and (3) neither curing nor supercritical CO_2 treatment as the control. Figure 1 shows the effect of supercritical CO_2 treatment on bending properties at various curing time of the CBP, neat cement boards (NC) and $Ca(OH)_2$ boards. We conclude that supercritical CO_2 treatment accelerates the curing process rapidly and enhances the mechanical properties of CBP. However, with a longer time span of treatment, the MOR and MOE values decreased and had a negative effect on board performance. It was considered that supercritical CO_2 treatment over a longer time span leads to degradation of CBP [2].

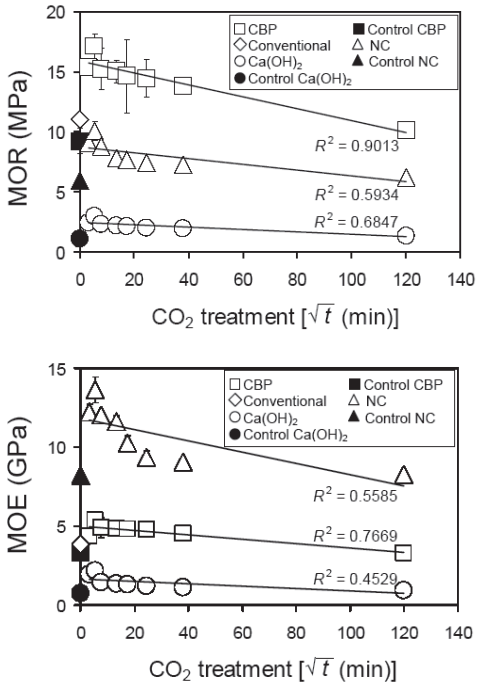

Figure 1. Effect of supercritical CO_2 treatment on bending properties at various curing time of the CBP, neat cement boards (NC) and $Ca(OH)_2$ boards.

We are expanding this research to *clarify* some factors which affect the properties of CBP using supercritical CO_2 treatment, and to estimate long term degradation of CBP in natural condition based on treatment of CO_2 to conventional cured CBP.

References

[1] Hermawan, D., Hata. T., Umemura. K., Kawai, S., Nagadomi, W., Kuroki, Y. "Rapid production of high-strength cement-bonded particleboard using gaseous or supercritical carbon dioxide", *J Wood Sci* 47:294-300, 2001

[2] Maail, R.S., Umemura, K., Aizawa, H., Kawai, S. "Curing and degradation processes of cement-bonded particleboard by supercritical CO_2 treatment", *J Wood Sci* 57:302-307, 2011

Novel Space Environment Monitor, Instrument, and Space Mission Concepts

(Laboratory of Space Systems and Astronautics, RISH, Kyoto University)

Hiroshi Yamakawa, Hirotsugu Kojima, and Yoshikatsu Ueda

Lorentz Force Spacecraft Formation Dynamics

Dynamics and control aspects of a charged satellite using the Lorentz force were investigated. The concept of the Lorentz-augmented charged satellite realizes propellant-less electromagnetic propulsion, using the interaction between an electro-statically charged satellite and the Earth's magnetic field. Charging of satellites can be controlled by devices like ion or electron gun. The devices are smaller and lighter than conventional chemical thrusters and suitable to be carried by small-size satellites. We investigated relative dynamics of two satellites orbiting around the Earth. One is a non-charged satellite called a target satellite, and the other is a charged satellite located near the target satellite on a circular orbit. We studied the effect of the Lorentz force on the relative motion of the chaser satellite with respect to the target satellite on an elliptic orbit or on a circular orbit as a special case.

Magneto-Plasma Sail (MPS) Space Propulsion System

An MPS (Magneto-Plasma Sail) is a unique propulsion system, which travels through interplanetary space by capturing the energy of the solar wind, which inflates a weak original magnetic field made by a super-conducting coil of about 2-10 m in diameter with an assistance of a high-density plasma jet. From our theoretical estimations, momentum transfer from the solar wind to a spacecraft with a coil is large enough if the plasma source is operated to inflate only the magnetic field away from the spacecraft. Our activities in 2006 are as follows: (a) Sizing (mass, dimension, current, etc.) of the super-conducting coil to produce magnetic field around the spacecraft, (b) Preparation of the experiment facility to measure magnetic field, temperature, current etc. around super-conducting coil.

Monitor system for Space Electromagnetic Environments (MSEE)

The main objective of the MSEE (Monitor system for Space Electromagnetic Environments) is to monitor the electromagnetic disturbances caused by human activities in space. It consists of the small sensor units distributed around the target space. Our main activities on the development of the MSEE in 2006 are as follows: (a) Development of the analogue ASIC containing the differential amplifiers and A/D converters, (b) Simulation study on the location estimation method for each sensor unit.

Wave-Particle Interaction Analyzer(WPIA) Instrument for Spacecraft Observation.

For a practical application of a plasma wave instrument, a direct measurement system of wave-particle interactions is one of the important systems to the space science mission. WPIA instrument can observe wave-particle interactions by calculation of the cross correlation functions between obtained waveforms and detected particles onboard. Our designed system is assembled in one FPGA (Field Programmable Gate Array) IC and data calibration and correlation method is programmed in FPGA.

Acceleration of the Molding Cycle of Semi-crystalline Polylactic Acid by Cellulose Nanofibers Reinforcement

(Graduate School of Agriculture, Laboratory of Active Bio-based Materials, RISH, Kyoto University)

Lisman Suryanegara

The main drawback of semi-crystalline type of polylactic acid (PLA) for industrial application is the longer injection molding cycles compared with conventional polymers such as polypropylene (PP). We found that the combination of nucleant addition and cellulose nanofiber reinforcement had a synergetic effect to accelerate the injection molding cycle of PLA.

Introduction

PLA has a great potential to replace petroleum-based plastics because of its high stiffness and strength. However, semi-crystalline PLA designed for semi-structural purpose has slower crystallization speed. Hence, when semi-crystalline PLA molding product at amorphous condition is subjected to above T_g, the product gives poor mechanical properties causing creep deformation as well as shrinkage due to crystallization.

Considering industrial applications, the slower crystallization speed of PLA resulting in longer molding cycle, is a significant drawback. The prolonged molding cycle in order to obtain fully crystallized PLA decreases productivity and increases the cost. Thus, the main objective of this study is to assess the possibility to accelerate the injection molding cycle of PLA by cellulose nanofibers reinforcement and nucleant addition. Our goal is to process PLA as productively as PP while keeping the advantage of mechanical reinforcement of cellulose nanofibers, which are the high thermo-mechanical properties.

Materials and Methods

To evaluate the effect of reinforcement, PLA and microfibrillated cellulose (MFC) at fiber content of 0, 3, 5, 10, and 20 wt% were mixed in an organic solvent. After the solution was dried at room temperature followed by vacuum-drying, a kneader was used to obtain a homogenous compound which was hot pressed. The melted samples were immediately quenched in liquid N_2 to bring them to a fully amorphous state. To obtain fully crystallized state, the amorphous sheets were annealed at 100 °C for 1 h. To attain samples with various crystallinities, the amorphous sheets at a fiber content of 10 wt% were annealed at 80 °C for different lengths of time. To evaluate the potential of MFC and nucleant in accelerating the injection molding cycle of PLA: PLA, phenylphosphonic acid zinc (PPA-Zn), and MFC at a fiber content of 10 wt% were mixed in an organic solvent followed by oven drying. The dry mixture were injection molded into different temperature mold and were kept in the mold for different lengths of time to obtain samples with various crystallinities.

The mechanical properties were studied by tensile test. The thermal properties were evaluated by TMA and DMA. The degree of crystallization was investigated by X-ray diffraction and differential scanning calorimetry.

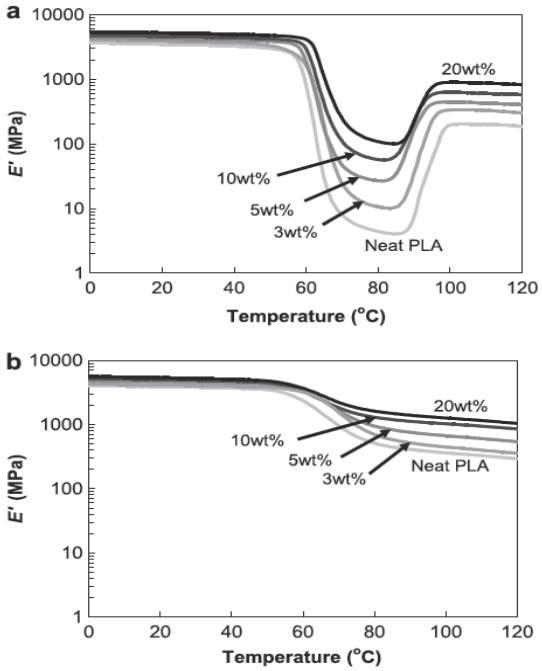

Fig. 1. Effect of MFC contents (wt%) on the temperature dependency of the storage modulus under (a) amorphous and (b) crystallized states

The deforming behavior of composites was performed by a cantilever beam test in a forced convection oven. Rectangular samples were clamped at one end as cantilevers and subjected to a temperature of 110 °C for 3 h.

Results and Discussion

Fig. 1 shows the effect of MFC reinforcement on the storage modulus of PLA in amorphous and fully crystallized states. In the amorphous state, the addition of MFC at a fiber content of 20 wt% improved the modulus of neat PLA by 50% from 3508 MPa to 5223 MPa at 20 °C (glassy state), and interestingly, by 27 times from 4 MPa to 109 MPa at 80 °C (rubbery state) [1].

Figure 2 shows the cantilever beam test of PLA and PLA/MFC 10 wt% composites with different degrees of crystallinity. The composite (Xc: 17%) did not show downward deformation during heating at 110 °C for 3 h. On the other hand, the amorphous composite (Xc: 0%) exhibited the highest downward deformation, which gradually decreased as the crystallinity increased up to 9%. The addition of fiber restricted the mobility of the polymer chains, and the presence of the crystalline structure of PLA also acted as a physical crosslinking, decreasing the mobility of the PLA amorphous regions, and as a result increasing the composite's stiffness [2].

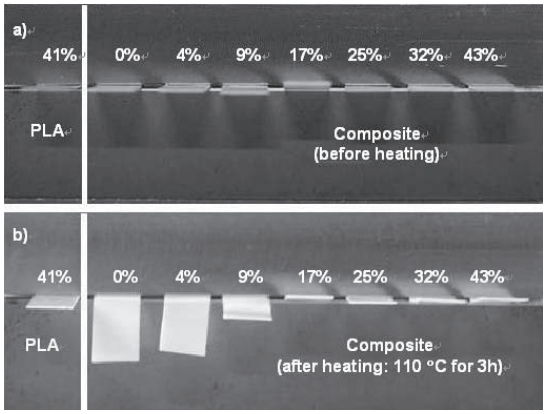

Figure 2. Cantilever beam test of PLA and PLA/MFC 10 wt% composites with different degrees of crystallinity at 110 °C for 3 h

Figure 3 shows samples shapes when ejected from the mold after holding at 95 °C for 10 s. Only the PLA/PPA-Zn/MFC composite could be obtained without distortion, while neat PLA and the PLA/PPA-Zn and PLA/MFC composites were all deformed. This result shows the advantage of MFC-reinforced PLA/PPA-Zn composite: although the composite was partially crystallized, it was easily demolded in a short time without distortion [3].

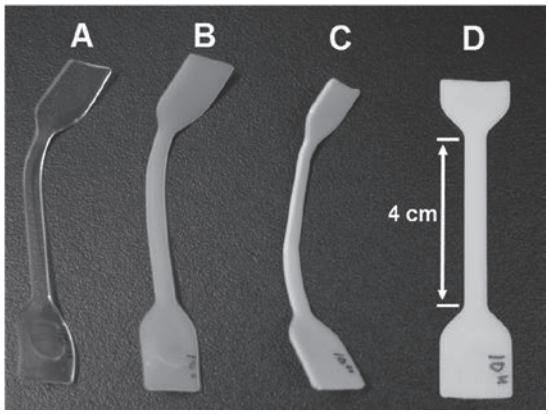

Figure 3. Samples shapes when ejected from the mold after holding at 95 °C for 10 s: a Neat PLA, b PLA/PPA-Zn, c PLA/

From these results, it was concluded that reinforcement with cellulose nanofibers made possible to manufacture high heat resistance and high strength the PLA semi-structural parts at similar molding cycles of PP. In the future, to apply this finding in industrial applications, a further experiment is needed to avoid the using of solvent method in the preparation of nanocomposites

References

[1] Suryanegara L, A.N. Nakagaito, and H. Yano, "The effect of crystallization of PLA on the thermal and mechanical properties of microfibrillated cellulose-reinforced PLA composites," *Compos Sci Technol* , vol. 69, no. 7-8, pp. 1187-1192, 2009.

[2] Suryanegara L, A.N. Nakagaito, and H. Yano, "Thermo-mechanical properties of microfibrillated cellulose-reinforced partially crystallized PLA composites," *Cellulose*, vol. 17, no. 4, pp. 771-778, 2010.

[3] Suryanegara L, H. Okumura, A.N. Nakagaito and H. Yano, "The synergetic effect of phenylphosphonic acid zinc and microfibrillated cellulose on the injection molding cycle time of PLA composites," *Cellulose*, vol. 18, no. 3, pp. 689-698, 2011.

Wood identification of cultural artifacts
－a combined use of synchrotron X-ray microtomography and optical microscopy techniques－

**(Graduate School of Agriculture,
Laboratory of Biomass Morphogenesis and Information, RISH, Kyoto University)**

Suyako Tazuru-Mizuno

Wood identification is an effective practice in the fields of archaeology, commerce, art history, architecture, and ethnological study, among others. The anatomical features of many wood species have been described for wood identification. In general, the identification of wood requires the observation of its microstructure from three directions: axial, radial, and tangential. One method involves the use of a razor blade to take a thin slice from the wood blocks and to then prepare microscopic specimens to determine the three directions. Although this method becomes simple after training and experience, it is not applicable in cases in which only a very small sample is available, as is always the case for wood works or artifacts that are part of the national heritage. Furthermore, the wood samples that have fallen off of such artifacts are often too brittle and soft because of their degradation as a result of biological attack or many other factors. Against this background, we can see that the development of alternative methods of identification is desirable. The requirements for such alternative means are that they must be nondestructive, rapid, accurate, and reproducible. A computed tomography technique (CT) is thought to be one of the best approaches. In the field of wood anatomy, CT has been used, but because the resolution is low, it is only applied to the investigation of tree rings. In this study, Synchrotron X-ray microtomography (μ-CT) at a synchrotron radiation facility (SPring-8), which is non-destructive of nature and has ultra high resolution (<0.5μm), was applied especially for the analysis of small and important artifacts (Fig 1).

In Chapter 2, the μ-CT, which makes possible the non-destructive investigation of 3D microstructures was applied to the identification of the wood of a historical wooden sculpture Seshin-bosatsu statue, a historical brittle wooden mask discovered in Kumamoto Prefecture, Japan (Fig 2), and old wooden sculpture Shinzo excavated from the Shiozuko site in Shiga Prefecture. These flaked samples of wooden cultural assets are quite small and compressed, and display insect damage and high moisture content. Using a μ-CT dataset, typical reconstituted slices from the three major directions of wood are prepared. Unlike optical micrographs, each reconstituted slice was only 0.5 μm thick, which made it necessary to increase the depth information. For this purpose, 24 slices were integrated to prepare pseudo-micrographs that were 12 μm thick using Image J software. This allowed us to apply wood anatomical features from the literature to the data obtained by synchrotron X-ray microtomography. Thus, Synchrotron X-ray microtomography methods have a tremendous potential. Because of its nondestructive character, the identified samples can be used further for chemical analysis, such as component analysis.

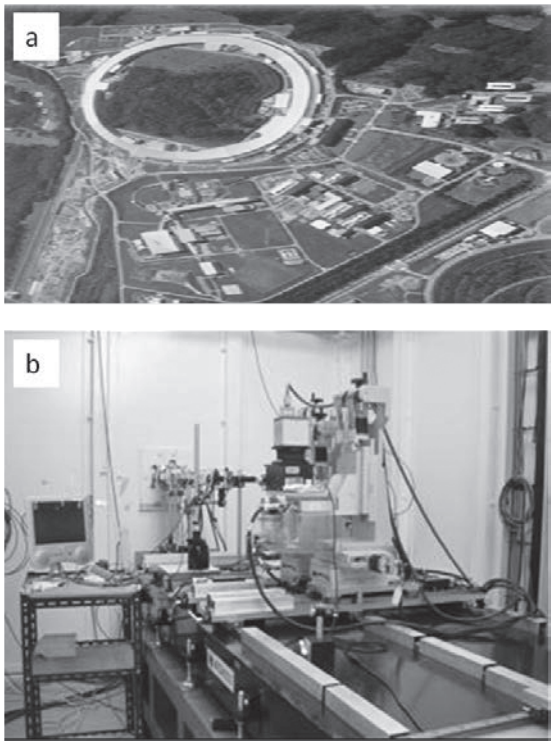

Fig 1: Bird-eye view of SPring-8 (a) and appearance of beam line 20XU (b).

In Chapter 3, wooden cultural assets that include many wooden sculptures were investigated in the same way. Recent study shows that in the 7th century, *Cinnamomum camphora* was basically used for wooden statues, while wooden statues of the 8th century were made of *Torreya nucifera*. However, for comparison with Buddha statues, the wood species and wood selection criteria used for Shinzo and Komainu have not thus far been adequately investigated. In Chapter 3, the author tries to identify wood species using synchrotron X-ray microtomography without causing any damage to the statues themselves. It is revealed that wooden statues of Shinzo and Komainu were mostly made of *Torreya nucifera* (Fig 3) and *Chamaecyparis obtusa*.

In Chapter 4, the author anatomically identifies the wood species in the Chion-in temple, Zuigenji temple, Myoutsuji temple, Yasaka shrine, Maruoka castle, Konchi-in tearoom, and Housyusya tearoom. Tiny samples from the disarticulation are useful for the identification of original wood. Wood identification is necessary not only in the investigation of original wood, but also in other research investigations, such as the value of a building, the purpose of an architectural feature, the transitions of building materials, and the regional characteristics of building materials. Moreover, wood identification has other significance for historical research. The books describing adequately the earliest construction work and restoration have sometimes been found. In order to confirm the descriptions of such historical data, wood identification also has a special meaning.

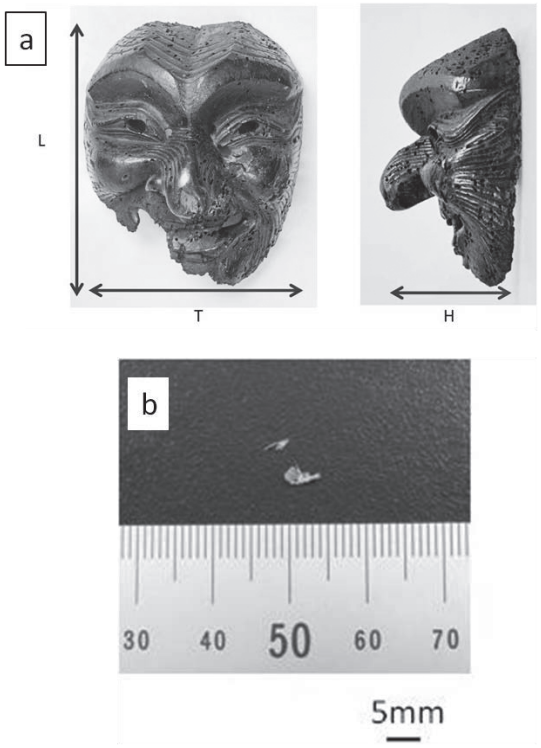

Fig 2: The old wooden mask (a) discovered at Yatsushiro city, Kumamoto, Japan. It was painted with black lacquer. (b) Small fragments were inevitably flaked off. Courtesy of Yatsushiro Municipal Museum.

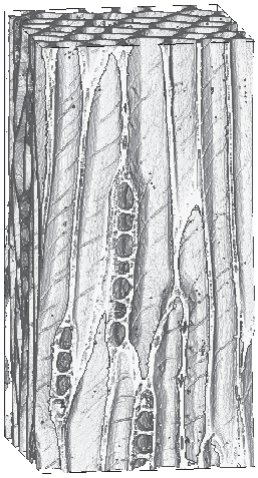

Fig 3: Typical 3D rendering of *Torreya nucifera* constructed using synchrotron microtomography dataset.

Wood identification is also effective in the field of archaeology. For example, determining tree species has helped us to understand the selection of wood in terms of wooden artifacts, vegetation, history, and other areas. Many and various woody remains have been excavated from many sites in Japan. Recently, the wood selected for several wooden artifacts in the past has been clarified by many scientists. Wood identification has also contributed to the determination of the wood selection process. In Chapter 5, the author identifies the anatomy of the wood species of about 400 woody remains originating from a shrine construction excavated from the Shiozu site (Heian era), Shiga prefecture. Based upon these identified results, the characteristics of wood selection used for shrine construction in the past environment of Shiga prefecture are discussed.

Acknowledgements

The author wishes to express her sincerest thanks to professor Junji Sugiyama, Research Institute for Sustainable Humanosphere, Kyoto University, for his kindest guidance and encouragement during the entire course of this study. The author wish to express special thanks to Shuichi Kawai, a professor at Research Institute for Sustainable Humanosphere Kyoto University and Keiji Takabe a professor at Kyoto University for their kindest guidance.

Involvement of auxin distribution in root nodule development of *Lotus japonicus*

(Graduate School of Agriculture, Laboratory of Plant Gene Expression, RISH, Kyoto University)

Kojiro TAKANASHI

Legumes (Fabaceae) constitute the third largest plant family with around 700 genera and 20,000 species. Legume plants form root nodules through symbiosis with a soil microbe called rhizobia. This plant-microbe symbiosis in nodules mediates a harmonized exchange of chemical signals between host plants and rhizobia. Nodules are biologically divided into two different groups, i.e., indeterminate nodules and determinate nodules. Indeterminate nodules, represented by *Trifolium repens* (white clover) and *Medicago truncatula*, are initiated from the inner cortex to form a persistent nodule meristem, which allows continuous growth, and leads to the formation of elongated nodules, whereas in determinate legumes, nodules are mostly developed from outer cortical cells and form spherical nodules.

Auxin is one of the most important regulators for nodule development. Since the possible involvement of auxin in nodule formation was first reported by Thimann, auxin distribution during nodulation has been studied in particular with indeterminate nodules. However, little is known about auxin involvement in determinate nodule formation. To evaluate auxin functions in the determinate nodulation of legume plants, I performed an auxin-responsive promoter analysis in detail. Using GH3:GUS transformed *Lotus japonicus*, detected auxin signals throughout the nodulation process, e.g., at the basal and front part of the nodule primordia, circumjacent to the infection zone of the young developing nodules, and at the nodule vascular bundle in mature nodules. I also investigated the effect of several auxin inhibitors, including newly synthesized auxin antagonist PEO-IAA on the nodulation of *L. japonicus*, and revealed that auxin was required for forming a nodule vascular bundle and lenticels (Fig. 1).

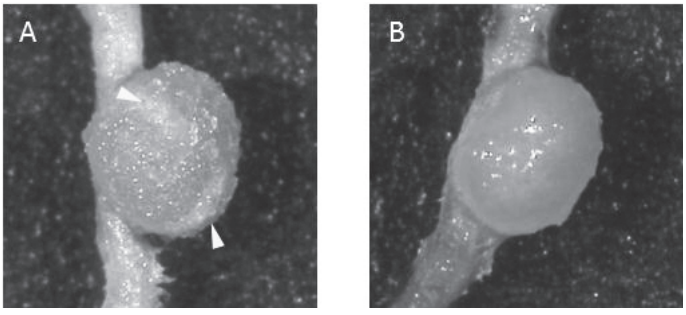

Figure 1. The effect of auxin inhibitor on nodule surface. (A) Typical mature nodule of *L. japonicus* at 21 dpi. Lenticels are pointed out by arrowheads. (B) The treatment of auxin inhibitor (NPA 100 μM) inhibited lenticel formation on the nodule surface.

In indeterminate legumes, auxin is accumulated at the site of rhizobia inoculation. This is caused by the inhibition of polar auxin transport by accumulation of flavonoids around the infection site, which are known

as regulators of auxin transport. When flavonoid biosynthesis is reduced by the gene silencing of chalcone synthase, which catalyzes the first step of flavonoid synthesis, *M. truncatula* was unable to inhibit polar auxin transport and resulted in reduced nodule number. A similar phenotype was observed when the auxin transporter gene was silenced. In addition, treatment of polar auxin transport inhibitors such as NPA and TIBA induce pseudonodule formation, suggesting that auxin accumulation is required for nodulation of indeterminate legumes. In contrast, the treatment of polar auxin transport inhibitors in determinate nodules did not induce a nodule-like structure, suggesting a different function of auxin between indeterminate and determinate nodules. It is, however, of interest to investigate the involvement of flavonoids in determinate nodule formation, because several genes in the flavonoid biosynthesis pathway are up-regulated at 2 dpi (days post inoculation) in *L. japonicus*.

Lenticels regulate gas permeability of nodules. Under low oxygen or waterlogged conditions, they develop more extensively, whereas they collapse, or develop very little during insufficient water conditions, or under high oxygen pressure. Because lenticel development on the nodule surface is accompanied with the nodule vascular bundle, growth regulators supplied from the vascular system likely facilitate lenticel development. Indeed, when the expression of two homeodomain proteins was suppressed, lenticel development was inhibited as well as the vascular tissues. My data suggests that auxin is necessary to form the nodule vascular bundle, and in fact, auxin itself is one of the candidates of growth substances that control lenticel formation. It is necessary to analyze mutants, which lack in lenticel formation, but can form a nodule vascular bundle, for clarification of further mechanisms of lenticel development.

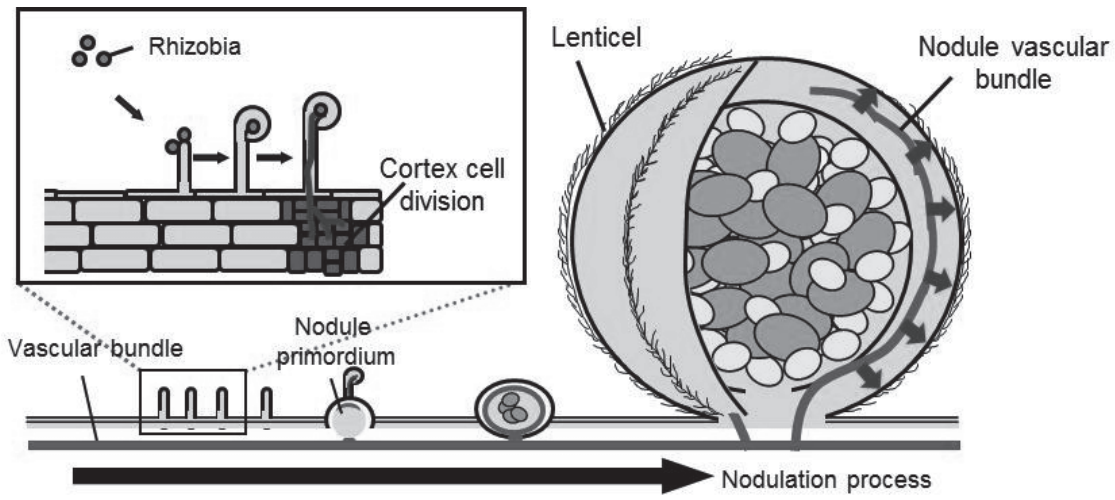

Figure 2. A model of determinate nodule development. Auxin is involvement in cortex cell division and nodule vascular development.

Observational study on diurnal precipitation cycle over Indonesia using 1.3-GHz wind profiling radar network

(Graduate School of Science, Laboratory of Radar Atmospheric Science, RISH, Kyoto University)

Yoshikazu Tabata

Variations in the diurnal precipitation cycle over equatorial Indonesia were investigated using 1.3-GHz wind profiling radars (WPRs) and rain gauges located at Pontianak (109.37E, 0.00S), Manado (124.92E, 1.55N), and Biak (136.10E, 1.18S). These WPRs were installed in the project of Hydrometeorological ARray for ISV-Monsoon AUtomonitoring (HARIMAU) on February 22, 2007, Setptember 18, 2009, and March 11, 2007, respectively.

WPR was originally designed to observe echoes from clear air turbulence. However, 1.3-GHz WPR is very sensitive to hydrometeor. Hence, in this study, the precipitation cloud type was classified from vertical profile of vertical beam Doppler velocity and spectral width observed by WPRs for each precipitation observed by rain gauges. At all three WPR sites, peak rain rate was detected during 1300-1500 LT by rain gauges. WPR observations showed that deep convective clouds were predominant during that period. At Biak, precipitation from midnight to morning was observed, whose dominant cloud types were both deep convective and stratiform. There was a clear difference in the afternoon-to-evening precipitation among the three WPR sites. Figure 1(a) shows the averaged diurnal rain rate for each cloud type at Pontianak. The peak rain rate was detected during 1400-1500 LT. During this period, the deep convective cloud type was predominant and accounted for more than 80% of the total rain rate. Figure 1(b) shows the frequency of precipitation for each cloud type. The frequency of deep convective type clouds increased from 1200 LT and reached a peak around 1500-1600 LT, which was similar to the result of the peak rain rate. There was a clear transition from the convective-type clouds to the stratiform-type clouds during 1500-2000 LT. The frequency of the stratiform-type clouds increased following the predominance of the deep convective type, and reached a peak during 1900-2000 LT. However, the stratiform rain rate was only about 0.2 mm/h. The afternoon-to-evening precipitation has the characteristics of a mesoscale convective system (MCS). Black

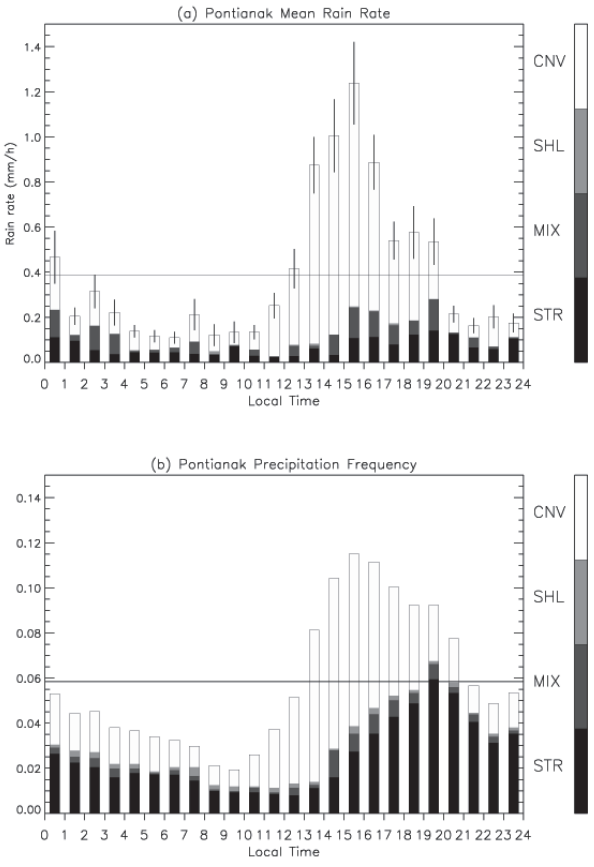

Figure 1. Diurnal cycle of (a) rain rate and (b) precipitation frequency at Pontianak as observed by WPR-gauge. For each precipitation event, the cloud type is classified as stratiform, mixed stratiform/convective, shallow convective, and deep convective types, which are indicated as STR, MIX, SHL, and CNV, respectively. Vertical lines indicate error bars of total rain rate defined by $\sigma/\sqrt{n}$. The horizontal lines in both panels indicate mean values.

body brightness temperature (Tbb) observed by MTSAT-1R satellite also indicated that the precipitation clouds had enough horizontal scale to be well organized as a MCS. At Manado and Biak, the peak rain rate in the early afternoon was characterized by a short period (within 3 h), and the precipitation after the convective precipitation was not clear.

Tbb data showed that the horizontal scale of cloud systems differs from Pontianak to Manado and Biak. The horizontal scale of the landmass around Pontianak is more than 100 km, while that of Manado and Biak is 10-100 km. The diurnal precipitation cycle was also investigated using 11 years of Tropical Rainfall Measuring Mission (TRMM) data. 3G68 grid data showed that the midnight to morning precipitation at Biak was caused by northward propagation of cloud system from northern coastal region of New Guinea Island. A 3G68 product with a horizontal resolution of 0.5 deg. could not resolve peak rain rate in the early afternoon at Manado and Biak, where convective clouds developed with the 10-100 km horizontal scale. Surface rain data with a horizontal resolution of 0.1 deg. were produced using the TRMM precipitation radar (PR) 2A25 product. This high-horizontal-resolution data set successfully detected the peak convective rain rate in the early afternoon at Manado and Biak. The rain rate peak was distributed in the land region of peninsula in Sulawesi Island, and the whole region in Biak Island.

The mechanism of diurnal precipitation cycle at Pontianak was further investigated. Around Pontianak, radiosonde and MTSAT-1R data showed that the zonal migration of each precipitation system was caused by zonal wind in the middle troposphere (in the altitude of 8-10 km). WPR echo intensity and spectral width clearly showed the development of the mixing layer in the daytime. Radiosonde observations at Pontianak revealed that water vapor showed a significant increase during 1000-1600 LT in the altitude of 1-4 km, and during 1300-1600 LT above 4 km. Minimum of water vapor around 1300 LT was observed below the altitude of 0.5 km. The upward atmospheric motion was frequently observed during 1000-1600 LT. The results showed that water vapor was transported upward by strong upward atmospheric motion in the daytime. The upward transport of water vapor is suggested to play an important role in the precipitation in the afternoon to evening at Pontianak.

At Pontianak, zonal wind variation was dominant below 1.5 km, which can be explained by sea-land breeze of Borneo (Kalimantan) Island. At Manado, zonal and meridional wind variation below 1 km can be explained by the sea-land breeze of Sulawesi Island, and the wind variation of meridional component in 1-3 km can be explained by return flow of sea-land breeze. At Biak, meridional wind variation below 2 km altitude was dominant, which can be explained by sea-land breeze of New Guinea (Papua) Island, not of Biak Island itself. At Biak, the diurnal variation of meridional wind was suggested to make a convergence in the lower troposphere, and acts an important role in northward propagation of precipitation system from northern coastal region of New Guinea Island. At all the three WPR sites, semidiurnal variation of zonal wind was observed in an altitude of 1-3 km, which is consistent with atmospheric tides. At Manado and Biak, upward atmospheric motion clearly increased in the daytime, which suggest that upward atmospheric motion plays an important role in the daytime precipitation.

The impact of intra-seasonal variation (ISV) to diurnal precipitation cycle was investigated. At all three WPR sites, peak rain rate and frequency in the afternoon were dominant in almost all MJO phases. The transition from convective clouds to stratiform clouds at Pontianak was clearly defined in almost all MJO phases. The precipitation from midnight to morning at Biak was dominant only in the active phase of MJO. The frequency of deep convective rain at three WPR sites did not show clear variation between active phase and inactive phase of MJO. On the other hand, the frequency of stratiform rain increased in the active phase of MJO.

The relationship between horizontal scale of landmass and precipitation feature from afternoon-to-evening was discussed based on this study and previous studies. In the case of landmass with a horizontal scale of less than 10 km, afternoon precipitation is not predominant. In the case of landmass with a horizontal scale of 10-100 km (like Manado and Biak), even though afternoon precipitation caused by localized convection occurs, cumulus convection is not well organized enough to produce a stratiform region after the peak of the deep convective rain rate. In the case of landmass with a horizontal scale of more than 100 km (like Pontianak), cumulus convection is well organized enough to produce a stratiform region of MCS in the afternoon to evening precipitation.

Study and Development of Microwave Irradiation Ports for Woody Biomass Pretreatment

**(Graduate School of Engineering,
Laboratory of Applied Radio Engineering for Humanosphere,
RISH, Kyoto University)**

Katsuyuki Yano

Pretreatment process is essential to produce bioethanol efficiency from woody biomass. We have been studying on a pretreatment system by microwave irradiation and have developed continuous-process type microwave pretreatment systems. The objective of the present thesis is development of highly efficient microwave irradiation ports for an effective woody biomass pretreatment.

Relative permittivity characteristics of solvents, which are mixed with the woody biomass, are important to design an efficient microwave irradiation port. The relative permittivity characteristics of water and ethylene glycol (EG) were measured as parameters of frequency and temperature, as shown in Fig.1 and Fig.2, respectively. We utilized the measured data to calculate reflection coefficient and design microwave irradiation ports.

In the continuous-process type microwave pretreatment systems, a glass plate was inserted into a microwave irradiation port in order to prevent microwave oscillator from high pressure. A dielectric cone was inserted on the glass plate in order to make the microwave reflection lower. We expressed the microwave irradiation port as equivalent circuit and we estimated reflection coefficient of the port. The calculation results were compared to 3D electromagnetic simulation results, as shown in Fig.3. The characteristic impedance of the dielectric cone can be expressed as equivalent relative permittivity.

We also developed a simple continuous-process type irradiation system, in which a magnetron is installed directly. The microwave irradiation port was designed as by the 3D electromagnetic simulator. We developed a prototype of the designed port and measured the temperature characteristics of reflection coefficient, when we assumed water as woody biomass mixture. From the measurement results, the reflection coefficient was lower than -9 dB at a frequency of 2.45 GHz when the water temperature was 15 C° to 70 C°. Finally, we succeeded to develop a simple and efficient microwave irradiation port.

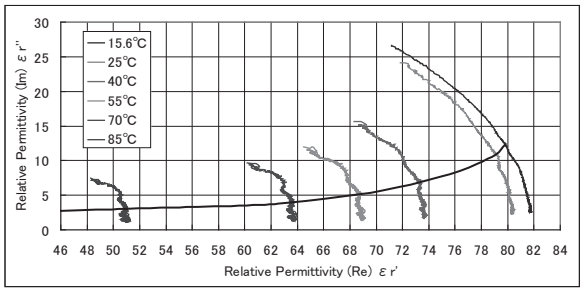

Fig.1 Characteristics of relative permittivity of water for the parameter of temperature.

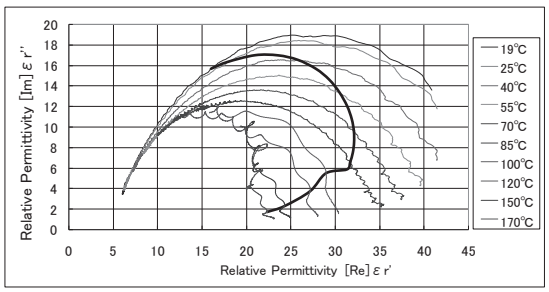

Fig.2 Characteristics of relative permittivity of EG for the parameter of temperature.

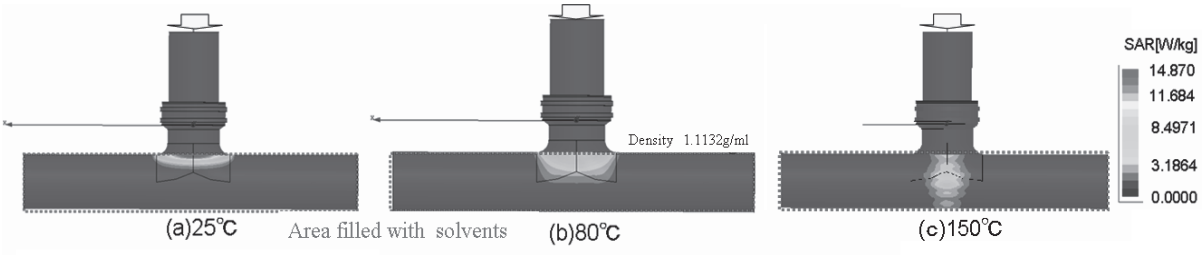

Fig.3 Simulation results of specific absorption rate.

Study and Development of a Microwave Wireless Power Supplying System for ZigBee Devices

**(Graduate School of Engineering,
Laboratory of Applied Radio Engineering for Humanosphere,
RISH, Kyoto University)**

Nozomu Suzuki

A wireless sensor network is a communication network system which consists of some sensor devices. The sensor network is adaptable to a wide variety of applications, for example, building automation and agricultural production management. Battery problems of a wireless sensor device including its lifetime and exchange cost are serious obstacles to constructing the wireless sensor network. The objective of the present thesis is to develop a ZigBee sensor network powered by external microwave, in order to realize a battery-less or wirelessly-charged wireless sensor network (Fig.1). We adopt the 2.4 GHz ISM band as a power transmission microwave frequency band. We first examined compatibility between microwave power transmission and ZigBee communication. We conducted ZigBee communication experiments while the ZigBee device was irradiated with external microwave. From the experimental results, we confirmed that the ZigBee devices can communicate in the external microwave at a frequency of 2.46 GHz. Therefore, we used 2.46 GHz as the power transmission microwave frequency. The external microwave power density which interrupts the ZigBee communications depended on received signal strength indicator (RSSI) of the ZigBee communication. Next, we developed a rectification circuit, and obtained a conversion efficiency of 65 %. Then, we developed a rectenna by connecting the rectification circuit to a power receiving patch antenna whose antenna gain was 6.35 dBi. We conducted power transmission experiments with the developed rectennas. When we used 4 rectennas, we obtained a conversion efficiency of 65 % and an output power of 64 mW, and confirmed that these rectennas could output enough voltage to operate the ZigBee device. Finally, we conducted ZigBee device operation experiments by microwave power transmission. The ZigBee device could be operated by microwave power, and could communicate with another ZigBee device. Using secondary batteries, we succeeded to operate a ZigBee device and charge the batteries at the same time (Fig.2).

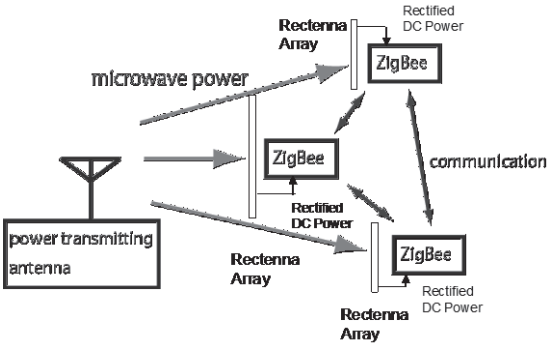

Fig.1 ZigBee sensor network with microwave power transmission.

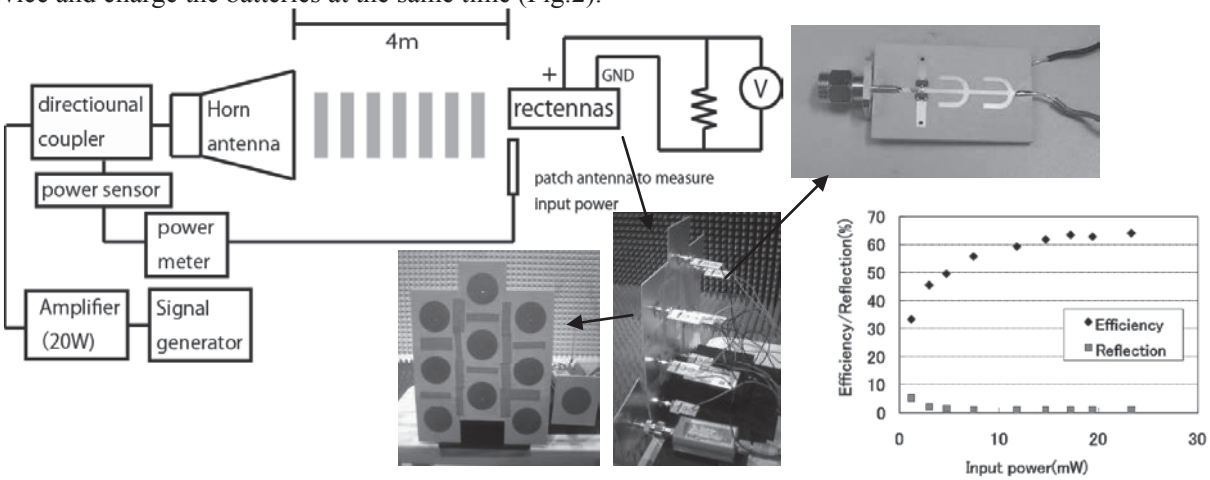

Fig.2 Experimental setup of ZigBee sensor network with microwave power transmission and RF-DC conversion efficiency of developed rectenna.

A Study on Data Distribution Characteristics of the GPS Radio Occultation Measurements

(Graduate School of Informatics, Laboratory of Atmospheric Sensing and Diagnosis, RISH, Kyoto University)

Naoto Yoshida

Global Positioning System (GPS) Radio Occultation (RO) is one of active remote sensing techniques. GPS RO employs a GPS receiver on board a low Earth orbit (LEO) satellite or an airplane to detect the occulted GPS radio signals passing through the atmosphere. GPS RO provides profiles of temperature, water vapor density and electron density, which are characterized by a good vertical resolution and high measurement accuracy. Since the first GPS RO experiment in 1995, a number of follow-on missions are carried out.

When planning a new GPS RO mission, the orbit of a LEO satellite is important, because the orbit decides characteristics of the GPS RO data distribution. While the data distributions of other satellite observations can be predicted directly by their satellite orbits, the GPS RO data distribution depends on the relative positions between the GPS and LEO satellites. In this thesis, we develop a numerical model for the GPS RO data distribution with realistic satellite orbital parameters.

A circular LEO satellite at a high inclination angle has been used in earlier GPS RO missions, since it provides a global data set. However, its spatial data distribution is non-uniform with respect to latitude. The high inclination angle LEO satellite leads to considerably smaller number of observation data in low latitudes. By contrast, a low inclination angle results in a concentration of data at low latitudes. Therefore, a combination of LEO satellites at different inclination angles can achieve the most uniform data distribution.

In addition, we sometimes need to get a uniform distribution with respect to local time, because many weather phenomena are dependent on local time. The data distribution versus local time has two peaks of the number of data in a day. The patterns of the data peaks depend on the right ascensions of ascending node of LEO satellites. A combination of LEO satellites with the right ascensions at equal intervals along 0-360 °may provide a uniform distribution as a function of local time.

Localized data distribution is also required to compensate for the lack of ground-based observations and get many observation data in important areas for atmospheric and ionospheric studies. The GPS RO measurements with geostationary and quasi-zenith satellites can provide the data distribution localized with respect to latitude and longitude. An equatorial orbit satellite can provide a data distribution concentrated in the equatorial region.

The airborne GPS Down-looking (DL) RO technique uses airplanes instead of LEO satellites. The airborne measurements can produce a lot of data in a particular region. If the measurements with many commercial flights are realized, we will get a lot of atmospheric profiles, for example over Japan.

Although we consider the ideal data distributions computed by the numerical model, data loss problems are often occurred in the real GPS RO missions. In the retrieval process from received signals to atmospheric profiles, many errors are caused at low latitudes and around East Asia. We suppose that the main causes of the errors are the ionospheric irregularities.

Considering that most of earlier GPS RO missions have used the LEO satellites at a high inclination angle and many data losses are occurred around the equator, the mission, which provides a data distribution localized at low latitudes, such as equatorial orbit satellites, is very important for future missions. The lack of data at low latitudes could be also compensated by attaching antennas to lateral or oblique sides of the LEO satellite and observing in the lateral direction relative to the satellite movement. Airborne DL RO is also a strong candidate for future missions, which could give a significant impact on the improvement of weather forecasts in a particular region.

New ceriporic acids with an unsaturated side chain produced by a selective white rot fungus, *Ceriporiopsis subvermispora*

**(Graduate School of Agriculture,
Laboratory of Biomass Conversion, RISH, Kyoto University)**

Midori Sasaki

A white rot fungus, *Ceriporiopsis subvermispora* is able to degrade lignin without intensive damage to cellulose. In selective white rot, lignin is degraded at a site far from the enzymes. The unique wood decay pattern suggests that extracellular low molecular mass metabolites are principally responsible for lignin degradation. To explain the lignin biodegradation by metabolites at a site far from enzymes, involvement of lipid peroxidation by chelated Mn^{3+} produced by manganese peroxidase (MnP) has been proposed. During wood decay, *C. subvermispora* secretes a series of unsaturated fatty acids including linoleic acid which can be oxidized by chelated Mn^{3+} to initiate the lipid peroxidaition. So far, four alk(en)ylitaconic acids; tetradecylitaconic (ceriporic acid A), hexadecylitaconic (ceriporic acid B), (*Z*)-7-hexadecenylitaconic (ceriporic acid C) and (*E*)-7-hexadecenylitaconic acid (ceriporic acid D) have been isolated and identified. An epoxidized ceriporic acid, (*R*)-3-(7,8-epoxy-hexadecyl)-itaconic acid has also been identified from the cultures of *C. subvermispora*. More recently, new analogues of alk(adi)enylitaconic acids have been found from the cultures of *C. subvermispora* by LCMS. However, their chemical structures have not been clarified. To elucidate the structure and functions of the new metabolites, alkenyl- and alkadienylitaconic acids were chemically synthesized. The synthetic compounds were identical to the metabolites found from the cultures of *C. subvermispora.* The alkadienylitaconic acid is a potential metabolite involved in the initiation of lipid peroxidation due to 1,4-dienyl structure in its side chain.

Acknowledgements
The author acknowledges Prof. M. Nakamura and Dr. H. Seike, Institute for Chemical Research, Kyoto Univ. for their valuable support and discussions.

Cellular response of a selective white rot fungus, *Ceriporiopsis subvermispora* to vanillin

**(Graduate School of Agriculture,
Laboratory of Biomass Conversion RISH, Kyoto University)**

Ayako Kido

Selective white-rot fungus, *Ceriporiopsis subvermispora* is able to degrade lignin without serious damage to cellulose. *C. subvermispora* secrets extracellular lignin-degrading enzymes including manganese peroxidase (MnP) and laccase (Lac). This fungus also secretes unsaturated fatty acids and lipid-related metabolites called ceriporic acids. In the selective white rot, lignin degradation by lipid peroxidation of unsaturated fatty acids and inhibition of cellulose degradation by ceriporic acids have been proposed as a key reaction for the selective ligninolysis. In lignin biodegradation by white rot fungi, vanillin has been found as one of the major degradation products from lignin. Previously it was reported that vanillin induced secretion of fatty acids, Lac and ceriporic acids by *C. subvermispora*. This suggests that vanillin may activate lipid metabolism by *C. subvermispora*. In the present study, cellular response of *C. subvermispora* to vanillin was analyzed by measuring fungal weight, activity of lignin-degrading enzymes and intracellular proteins expressed in the fungal cultivation. In the presence of vanillin, increase in fungal weight and laccase production was found. Two-dimensional electrophoresis coupled by in-gel tryptic digestion and MALDI-TOF MS revealed detailed profiles of the proteins up-regulated or down-regulated in response to the vanillin administration.

Expression and functional analysis of a gene encoding dicarboxylic acid methyltransferase from a selective white rot fungus, *Ceriporiopsis subvermispora*

**(Graduate School of Agriculture,
Laboratory of Biomass Conversion RISH, Kyoto University)**

Kohei Kitaaki

Selective white rot fungus, *Ceriporiopsis subvermispora* is able to degrade lignin without intensive damage to cellulose. The unique wood decay pattern implies that the extracellular low molecular mass metabolites are principally responsible for the lignin degradation. Alk(en)ylitaconic acids, ceriporic acids have been found as a major extracellular metabolite of *C. subvermispora*. A series of ceriporic acids with different side chain structures have been found and chemically synthesized. Ceriporic acids suppress cellulose degradation by inhibiting reduction of ferric ion. Recently, it was suggested that *C. subvermispora* produces monomethyl ester of ceriporic acids. Purpose of the present study is to identify the enzyme which catalyzes methyl esterification of ceriporic acids.

trans-Aconitate methyltransferase is an enzyme which catalyzes esterification of *trans*-aconitic acid from *S*-adenosylmethionine (SAM). It is known that some *trans*-aconitate methyltransferases exhibited a wide range of substrate specificity including itaconic acid. Therefore, *trans*-aconitate methyltransferase gene (*Cs-tam*) was cloned from *C. subvermispora*, expressed in *Escherichia coli* and substrate specificity of the expressed protein, *Cs*-Tam was analyzed. Purification on a Ni-affinity column and analysis with SDS-PAGE and MALDI-TOF-MS revealed successful expression of *Cs*-Tam in *E. coli*. To analyze the enzyme activity, lysate of recombinant *Cs*-Tam was incubated with itaconic acid in the presence of SAM. GC/MS analysis demonstrated that *Cs*-Tam esterified itaconic acid to its 4- and 6-monomethylester. Substrate specificity of the recombinant *Cs*-Tam to ceriporic acids was also analyzed by LCMS.

3D-reconstruction of Cellulose Synthase by Electron Microscopy

**(Graduate School of Agriculture,
Laboratory of Biomass Morphogenesis and Information, RISH, Kyoto University)**

Ami Sugano

Cellulose is one of the major biomass on the earth, and billions tons of that are produced a year by many biological organisms. This is because cellulose has strong mechanical strength and biological resistance, which are given by its high crystalline fibrous structure rich with hydrogen b onding network, microfibril. The gene of cellulose synthase is identified in many species, but none of them is proven to be the molecule that synthesizes cellulose microfibril. It's because the cellulose synthase is membrane protein and forms complex. As a simple model, vinegar-producing bacterium, *Gluconacetobacter xylinus* is selected. It is shown in this organism that two proteins are necessary to synthesize cellulose *in vitro*: GxCesA and GxCesB. Then, this study focused on these proteins and aimed to analyze these structures.

Experiment

GxCesA and GxCesB protein were coexpressed by *E.coli* expression system, which was designed to have GxCesB with His6 tag fused at carboxyl terminal. Cell membrane was isolated from the grown *E. coli* cells expressing GxCesA and GxCesB by differential centrifugation, and solubilized by detergent to have these two proteins in extract. The solubilized fraction was purified by metal affinity and gel filtration chromatography. In the current protocol, it is not possible to purify both GxCesA and GxCesB as the former was lost during the purification steps, and as a result highly purified GxCesB was obtained. This sample was observed by TEM (Transmission Electron Microscopy) with negative staining. The specimen was micrographed at 0° and 45° as a tilt-pair, and analyzed with SPIDER [1] and EMAN [2] package.

Results

Purified GxCesB protein was estimated to be 1,000 kDa by gel filtration chromatography, indicating that GxCesB is 10-12mer of homo-oligomer. By electron microscopy with negative staining, GxCesB was consistently observed as globular particles of 15 nm. As there has been no structural information about this protein, we tried to reconstruct three dimensional structure of GxCesB by random conical tilt using a series of tilt-pair. When alignment of the particle images was carried out by reference-free method, less features were found in the model as shown in Figure 1A, which may result from incorrect alignment and/or assignment of angular information. On the other hand, heterogeneous features are found in the model reconstructed from the images that were aligned by multi-reference alignment (Figure 1B). Starting from each of these 30 structures, we respectively refined model with 1136 particles using EMAN. The refined model has a kind of heterogeneity, and it became clearer when 2-fold symmetry was applied: the face that has "horns" (top) is found in the opposite to the flat face (bottom). This feature appeared whichever the initial structure was selected for the refinement, suggesting that both purification and reconstruction (image analysis) were reliable enough for further analysis.

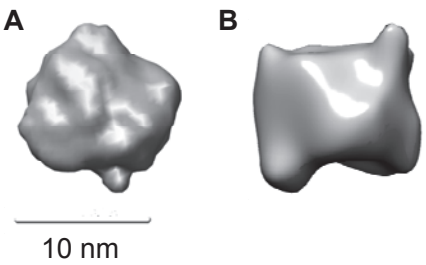

Figure 1. Three dimensional models of GxCesB reconstructed in this study by random-conical tilt: (A) a model when alignment was done by reference-free and (B) multi-reference protocol. Both models are shown with the noise-less level, by which *ca*. 70-80% of the volume expected from 1,000 kDa of MW was explained.

Acknowledgements

The author appreciates Associate Prof. Kenji Iwasaki (IPR, Osaka University) for guiding to the calculation of 3D structural model with single particle analysis.

References

1. **http://www.wadsworth.org/spider_doc/spider/docs/spider.html**
2. **http://blake.bcm.tmc.edu/eman/**

Functional Analysis of Expansin with Infrared Spectroscopy

**(Graduate School of Agriculture,
Laboratory of Biomass Morphogenesis and Information, RISH, Kyoto University)**

Masato Naruse

Expansin is cell wall protein that plays an important role for expansion growth of the plant cell and remodeling of cell wall. It is thought that expansin relaxes the cross-link by hydrogen bonds between cellulose and hemicellulose/cellulose in cell wall, which results in loosening and allowing the wall to be expanded by turgor pressure. Interestingly, molecule of expansin is a glycosylhydrolase of GH-45 family although it does not have no hydrolyzing activity of glucan. To understand the mechanism of expansin, we have used infrared spectroscopy together with intracrystalline deutrated cellulose as a substrate.

Experiment

In order to selectively see the hydrogen bonding in cellulose crystal, we prepared deutrated cellulose by hydrothermatl treatment with $NaOD/D_2O$ system. Cellulose from marine algae *Valonia* was selected as its large crystallite size allows spectroscopic changes to be easily detected when hydrogen bonding is disturbed in light water. A bacterial homologue of expansin EXLX1 is heterogously expressed with hexa-histidine tag fused at C-terminal by *E. coli*. The recombinant EXLX1 was purified by Ni^{2+} affinity chromatography. The deutrated cellulose was precisely measured to prepare 1 mg/mL suspension in 50 mM citrate buffer (pH4.8), and treated by 0.2 mg/mL of the purified EXLX1 at 45°C for 24h. For clearly seeing OD/OH exchange in cellulose, EXLX1 was thoroughly removed by washing with 0.1 N NaOH solution. FT-IR measurement was done with microscopic mode (Figure 1), and about 200 spectra were collected from different places in each specimen. The ratio between OD- and OH-signal (OD/OH) was calculated from the spectra, and compared with each other by statistical test.

Results

The author showed that a bacterial homologue of expansin EXLX1 decreased OD/OH ratio in the deutrated crystalline cellulose. This can mean OD/OH exchange in crystalline cellulose as previously hypothesized [1]. As well however, it was shown that BSA also decreased the ratio although smaller change. Then the author conducted the same experiment with lost-function mutant of EXLX1. When the residue of EXLX1 corresponding to catalytic acid in HiCel45A (endoglucanase V of *Humicola insolens*) [2] is mutated to Asn, the decrease of OD/OH was not observed. This result supports that (i) the observed decrease of OD/OH in crystalline cellulose results from the action of expansin itself and (ii) the mechanism of this activity may be substantially same as that of inverting-type hydrolases. Although the author tried to correlate this spectral change with the degree of enhancement of cellulase reaction, the consistent interpretation seems difficult. More detailed studies are definitely necessary to know what the decrease of OD/OH means and subsequently understand the mechanism of expansin for cellulose/hemicelluloses or cell wall.

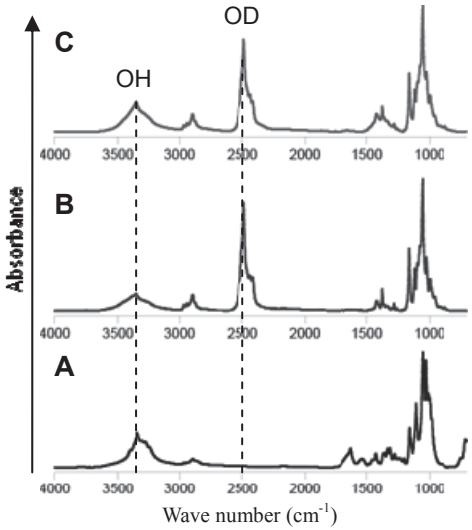

Figure 1 Infrared spectra from purified *Valonia* cellulose (A), its intracrystalline deutrated cellulose (B) and EXLX1-treated deutrated cellulose (C).

Acknowledgements

The author appreciates Drs. Katsuro Yaoi and Ken'ichiro Miyazaki from AIST for collaborative work.

References

1) S. McQueen-Mason and D. Consgrove *Proc. Natl. Acad. Sci.* **91**, 6574-6578 (1994)
2) G. J. Davies *et al. Biochemistry* **34**, 16210-16220 (1995)

Study on Formation Process of Relativistic Electron Flux Through Interaction with Chorus Emissions in the Earth's Magnetosphere

(Graduate School of Engineering, Laboratory of Omura, RISH, Kyoto University)

Masato Yoshikawa

We perform test particle simulations of energetic electrons interacting with whistler-mode chorus emissions in the radiation belt. We assume a pair of chorus elements propagating northward and southward along the magnetic eld from the equator. The variation of the wave amplitude and frequency is determined by the nonlinear wave growth theory. By tracing trajectories of many particles of the same energy and pitch angle with different phases and locations along the magnetic field line, which forms a delta function in the energy and pitch angle phase space, we obtain numerical Green's function as a function of energy and pitch angle. We varied the energy and pitch angle over ranges 0:01 - 6 MeV and 10 - 90◦ respectively to obtain a set of Green's functions, showing efficient acceleration processes of the relativistic turning acceleration (RTA) and the ultra-relativistic acceleration(URA). Assuming the initial distribution function of energetic electrons (< 30 keV), we perform a convolution integral with the Green's functions numerically to find a variation of the distribution function in the phase space after the nonlinear inter-action with a pair of chorus elements. By repeating the convolution integral many times, we can follow a time evolution of the distribution function interacting with a sequence of the chorus elements occurring repeatedly in time. Rapid formation of relativistic electron ux is achieved through RTA and URA due to chorus emissions, while resonant particles in the lower energy range less than 100 keV are scattered to lower pitch angles resulting in precipitation to the polar atmosphere. In the pitch angle distribution function, we _nd a pancake type in a lower energy range (< 1:5 MeV) and a buttery type in a higher energy range (1:5 - 2:5 MeV). A long time evolution of the energy distribution function shows a plateau formation in an energy range of 1-2 MeV. The time scale of formation of relativistic electron ux is much shorter than that predicted by the quasi-linear diffusion model.

Effects of soil treated with a nonrepellent insecticide, fipronil at low concentrations on subterranean termites

(Laboratory of Innovative Humano-Habitability, RISH, Kyoto University)

Yuichi Yamamoto

Chemicals that do not repel termites from penetrating into treated soil but rather successfully kill them are called nonrepellent termiticides, and they have been accepted worldwide as new-generation alternatives to conventional soil-poisoning repellent termiticides. The success in termite management depends on the lack of a repellent effect and the slow-acting characteristics of these termiticides may allow transfer of toxicants between exposed and unexposed termites through their social behaviors such as trophallaxis and grooming The transfer of a toxicant (fipronil) is thought to cause the elimination of termite colonies. The main aim of the present research was to determine the effect of treatment concentrations and presence of dead termites on the tunneling of subterranean termites in the laboratory. Termite bioassay was conducted at concentrations of fipronil [0-50 ppm (w/w soil)] lower than manufacturer's specifications.

Materials and methods

Soil-penetration test: A glass tube filled with treated and untreated soil (or 20 dead termite bodies), agar was used as a test device. Termites (50 workers + 5 soldiers of *Coptotermes formosanus* Shiraki) were placed at the bottom of the tube, and were forced to penetrate up to a wood piece (Fig. 1). Test soil was treated with fipronil (a commercial product) at 0 ~50 ppm.. Penetration distance, wood consumption and termite mortality were determined after one-week bioassay at 28 ± 2 ºC and 80% RH. Repellency to dead bodies was tested, when 20 dead bodies that were prepared by freezing, exposure to the toxicant or microbial degradation were placed beneath the treated soil.

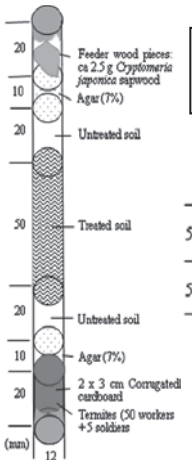

Fig. 1 Assembled unit for soil-penetration test

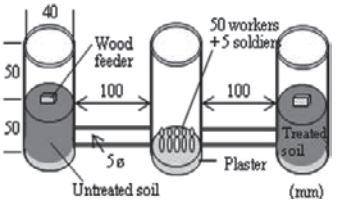

Fig. 2 Assembled unit for soil-choice test

Soil-choice test: An acrylic pipe was used as a test chamber (Fig. 2). Fipronil concentrations in the treated soil ranged from 0 to 50 ppm. The effect of accumulation and occurrence of dead bodies was tested when 50 dead termites were mixed with untreated soil and 10 bodies prepared by freezing process were placed around a wood feeder on the treated soil, respectively. Fifty workers and 5 soldiers were released in the central chamber. Test units were maintained for two weeks under the same condition of soil-penetration test. Measurement items were the same as well.

Results and discussion

Soil-penetration test: Penetration distances at 5 and 50 ppm were significantly shorter than 0 and 0.1 ppm. Worker termites succeeded in passing through the zone with dead bodies, regardless of preparatory processes of dead bodies.

Soil-choice test: Termites could not reach wood feeders at any treatment concentration.(>0.1 ppm). Termites aggregated in the central chamber within one day after the initiation of bioassay, and they would not.move afterwards. This was regarded as repellency of termite to dead bodies.

In both tests to determine the effect of accumulation and occurrence of dead bodies, repellency was observed, although termites penetrated through the treated soil zone. When a group of termite once aggregated in the treated chambers, and microbial growth on the dead bodies was subsequently seen, they moved towards the central chamber and finally were dead within a few days. Since the test design did not allow termites to clean up dead termites outside their foraging territory, further simulation tests should be done.

Improvement of the effectiveness of bait technique by liquid attractants and arrestants in termite management

(Laboratory of Innovative Humano-Habitability, RISH, Kyoto University)

Naotaka Maru

Although the bait-application is well known as an environmentally sound method of subterranean termite management, both difficulty in discovering baits by termites and low termite-arrest on baits have been critical for successful termite management. The use of attractants and arrestants is thought to improve the baiting program. The object of this study was to evaluate sports drinks and their derivatives as attractants and/or arrestants for improving the effectiveness of bait technique against subterranean termites.

Materials and Methods

Sports drinks and preparation of their derivatives: Five commercial sports drinks (A, B, C, D, E) were chosen by their ingredients. Four sports drinks (A, B, C, E) without phosphate were mixed with ammonium dihydrogenphosphate (P), and three sports drink derivatives and one sports drink (AP, BP, D, EP) without sugars were prepared by mixing with sucrose (S) for filter-paper choice-test. Three treatment concentrations (1/1, 1/5, 1/10) were prepared by diluting sports drinks with distilled waters for soil choice-test. Seven treatment liquid samples (A:1/1, A:1/5, A:1/10, B:1/10, C:1/5, E:1/5, E:1/10) were additionally prepared by mixing with ammonium dihydrogenphosphate.

Choice-test using filter paper: A filter paper was divided into quarters and two each of them were treated with sports drinks or modified liquid samples and distilled water, respectively. Each of these papers was placed on a petri dish. Thirty workers and three soldiers of *Coptotermes formosanus* Shiraki were introduced in the central petri dish. The number of termites present in treated and untreated areas was counted at regular intervals. After 5 days, consumption of filter papers was calculated.

Choice-test using soil: Three acrylic cylindrical containers were connected by acrylic tubes. A bottom of center container was formed by plaster, and two side containers were placed inside petri dishes. Soils were mixed with an individual treatment liquid sample and distilled water and put into side containers, respectively. Wood blocks were placed on the soil surface. One hundred workers and ten soldiers of *C. formosanus* were introduced into the center container. After three weeks, consumption of wood blocks was determined and the number of termites present in each container was counted at the end of test.

Result and Discussion

Choice-test using filter paper: Treated filter papers were consumed equally to or more than untreated ones except for DS. Significantly higher consumption was seen in the following cases: A, C, AP, CP, EP, P and EPS. The number of termite on treated filter papers was greater than on untreated ones in some cases. The addition of phosphate seemed to enhance the consumption of filter papers and termites arresting. In contrast, the addition of sucrose was not always favorable for attraction and arrest/aggregation of termites on the treated filter paper.

Choice-test using soil: It was clearly shown that consumption of the wood blocks was significantly greater in the container treated with C (1/5), D (1/10), AP (1/1), AP (1/5) and CP (1/5) than in untreated container ($P<0.05$). The number of termites was significantly greater than in the container treated with B (1/1), C (1/1), D (1/1), AP (1/1) and CP (1/5) than in untreated container ($P<0.05$). Attractant and/or arrestant effects of each treatment sample on *C. formosanus* were varied with dilution rates, and the addition of phosphate increased these effects in some cases.

Conclusion

These results suggested that when potential sports drinks are selected, applied at appropriate concentrations and mixed with co-agents such as phosphate, it is quite possible that they are thought to contribute to the increased effects as attractants and arrestants.

Characterization of *Oryza sativa* caffeate *O*-methyltransferase

(Graduate School of Agriculture, Laboratory of Metabolic Science of Forest Plants and Microorganisms, RISH, Kyoto University)

Norie Hirose

The low efficiency in the enzymatic saccharification is attributed to the fact that lignin tightly covers cellulose and hemicelluloses which are the substrates for hydrolases. Therefore, the regulation of lignin biosynthesis in biomass plants would improve the yield of the enzymatic saccharification. In this context, the elucidation of the biosynthetic mechanism of lignin biosynthesis in biomass plants is important.

Lignin is biosynthesized via the cinnamate/monolignol pathway. The pathway in dicotyledons has been extensively studied thus far. In contrast, the pathway in monocotyledons has not been well understood. Monocotyledons include important biomass plants such as switchgrass, erianthus, miscanthus, and sorghum classified as Gramineae. In this study, the author characterized a caffeate *O*-methyltransferase, a key enzyme involved in syringyl lignin biosynthesis in the cinnamate/monolignol pathway using rice, a model plant of Gramineae, and examined the increase of the saccharification by knock-down of the gene expression.

First, the author conducted the biochemical characterization of a rice *O*-methyltransferase (COMT3). Recombinant COMT3 was expressed in *E. coli* and purified as a His-tagged protein. The protein was reacted with various possible substrates, such as caffeic acid, 5-hydroxyferulic acid, caffealdehyde, 5-hydroxyconiferaldehyde, caffeyl alcohol, and 5-hydroxyconiferyl alcohol. After trimethylsilyl derivertization, the products were analyzed on GC-MS. V_{max}, K_m and k_{cat} values for each substrate (10-150 μM) were determined. As a result, COMT3 was found to catalyze *O*-methylation of all substrates. Among these substrates, 5-hydroxyferulic acid and 5-hydroxyconiferaldehyde showed smaller K_m (22 and 26 μM, respectively) and larger k_{cat} K_m^{-1} (478 and 294 μM^{-1} min^{-1}, respectively) than those of the other substrates, suggesting that the two substrates are the best two for COMT3 in this study. Furthermore, COMT3-mediated *O*-methylation of 5-hydroxyferulic acid was strongly inhibited by 5-hydroxyconiferaldehyde (competitive inhibition, K_i 2 μM), while that of 5-hydroxyconiferaldehyde was not inhibited by 5-hydroxyferulic acid. A substrate inhibition was observed when the concentration of 5-hydroxyconiferaldehyde was higher (25-150 μM). Interestingly, when 5-hydroxyferulic acid was added to the reaction mixture, the substrate inhibition was mitigated. Taken together, the results indicate that 5-hydroxyconiferaldehyde was preferentially methylated by COMT3 compared to 5-hydroxyferulic acid, strongly suggesting the pathway for syringyl lignin biosynthesis from coniferaldehyde to sinapyl alcohol *via* 5-hydroxyconiferaldehyde and sinapaldehyde in rice.

Second, the author conducted the characterization of COMT3-downregulated rice by RNA interference (RNAi) to examine the function of COMT3 *in vivo*. The T1 population of *COMT3* RNAi lines of rice plants was cultivated in a 3-L plastic container containing a nutrient solution in a growth chamber. The plants were submitted to quantitative reverse-transcriptase PCR (qRT-PCR) analysis of the gene expression, lignin staining, thioglycolic acid lignin analysis, and enzymatic saccharification. qRT-PCR analysis revealed that the expression of *COMT3* RNAi lines were strongly suppressed compared with wild type in all organs tested (leaf, sheath, and stem), indicating that the RNAi of *COMT3* in rice was successful. In Wisner staining, cortical fibers and vascular bundles were stained dark red in wild type, but were stained light red in the RNAi lines, suggesting that a decrease in lignin quantity in the RNAi lines. Thioglycolic acid lignin analysis showed that in wild type, lignin contents ranged from 14.9 to 22.6 %, whereas those in the RNAi lines, ranged 7.2 to 16 %, and these of all parts were decreased compared with wild type. The saccharification efficiencies of RNAi lines increased 2 to 12.2 % compared to wild type.

Taken together, this study strongly suggests the COMT3 preferentially catalyzes the formation of sinapaldehyde from 5-hydroxyconiferaldehyde and is involved in lignin biosynthesis, and the COMT3 down-regulation is effective for the increase of the efficiency of saccharification of rice straw.

Characterization of MATE-type transporter involved in alkaloid transport in *Nicotiana tabacum*

(Laboratory of Plant Gene Expression, RISH, Kyoto University)

Shingo Ito

Alkaloids play a key role in the defense mechanism in plants to protect themselves from pathogens and herbivores. The major alkaloid of the *Nicotiana* species, nicotine, is translocated via xylem transport from the root tissues where it is biosynthesized to the accumulation sites, the vacuoles of leaves. However, its transport mechanism is still largely unknown. Recently, our transcriptome analysis of methyl jasmonate-elicited tobacco BY-2 cells identified four transporter genes (Nt-JAT1, C215, T408, T449) which were highly up-regulated in a coordinate manner with the nicotine biosynthetic genes.[1)] Characterization of Nicotiana tabacum jasmonate-inducible alkaloid transporter 1 (Nt-JAT1), belonging to the family of multidrug and toxic compound extrusion (MATE) transporters, showed that this protein was expressed in roots, stems, and leaves, and localized in the tonoplast of leaf cells. Biochemical analyses showed that Nt-JAT1 functioned as a nicotine/proton antiporter. Furthermore, we analyzed other MATE-type transporters such as C215. The possible role of these transporters in nicotine translocation is discussed.

1) Morita M et al. (2009) PNAS 106: 2447-2452

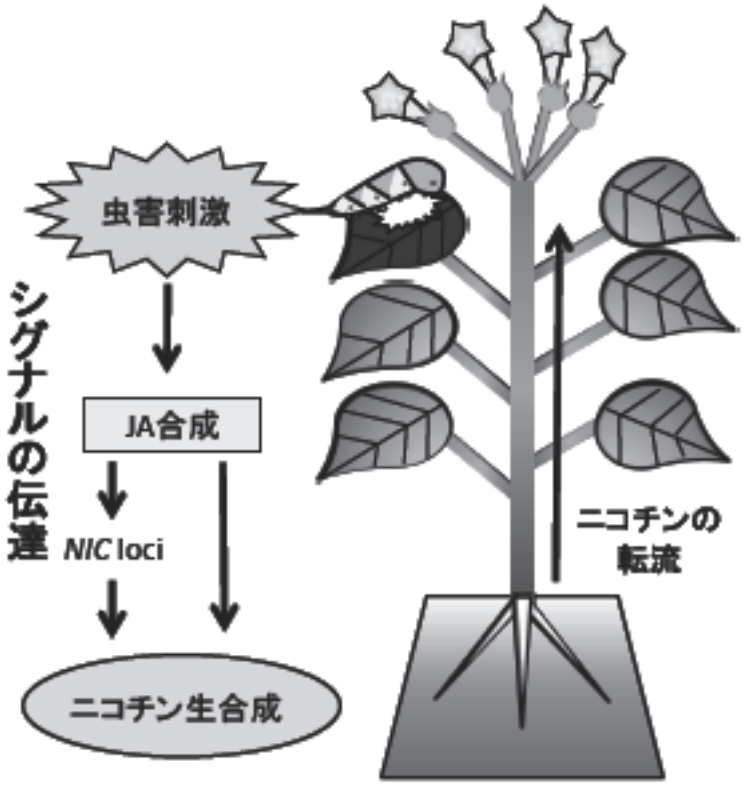

Specific accumulation of prenylated flavonoid in a tropical tree *Macaranga tanarius* grown in Okinawa

(Laboratory of Plant Gene Expression, RISH, Kyoto University)

Yoko Maeda

Propolis is a natural resinous product collected by honeybees from certain plants. It has gained popularity as a food and alternative medicine. However biological activities of propolis largely differ according to the area where it is produced because honeybees choose different plant species depending on the area. Among various lots of propolis, that of Okinawa contains characteristic prenylflavonoids that are not seen in other regions such as Europe and Brazil. These compounds are geranylated eryodictiol derivatives (see structures below). In the previous work of Dr. S. Kumazawa of Shizuoka Prefectural University, the plant origin of okinawan propolis was identified as a tropical tree species, *Macaranga tanarius* (Euphorbiaceae). Honeybees scraped white resinous material from the surface of plant fruits of *Macaranga tanarius* and brought it back to their hive to use it as propolis.

In this study we have found that the resinous materials developed on the surface of *M. tanarius* fruits are glandular trichomes and they are specific tissues, in which prenylated flavonoids are accumulated, as prenylated flavonoids are almost undetectable in the fruits from which the white glandular trichomes are removed.

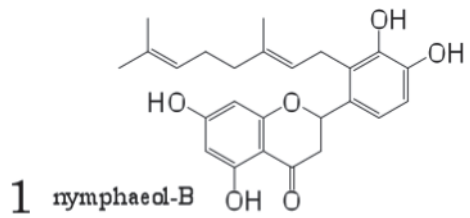

1 nymphaeol-B

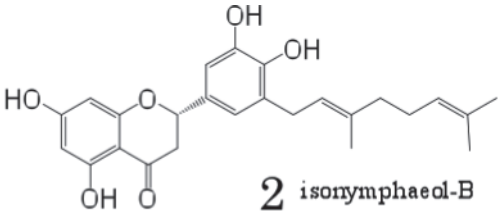

2 isonymphaeol-B

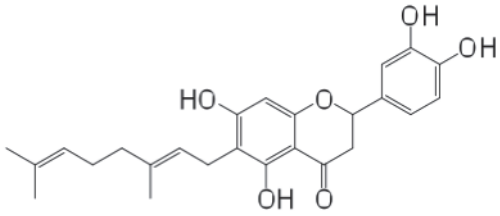

3 nymphaeol-A

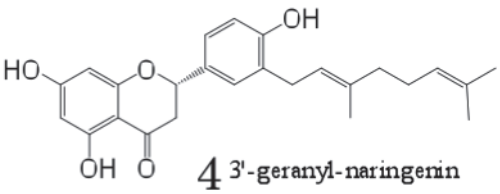

4 3'-geranyl-naringenin

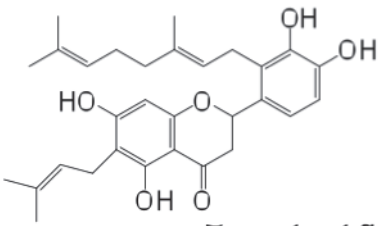

5 nymphaeol-C

Assessment of radar reflectivity factor and Doppler velocity measured by portable X-band and Ka-band Doppler weather radars

**(Graduate School of Informatics,
Laboratory of Radar Atmospheric Science, RISH, Kyoto University)**

Nobuyuki Ikeno

New X-band Doppler weather radar (XDR) has been developed to monitor localized torrential rains and tornadoes. XDR has the portability to be carried by a cart, and has high cost performance attained by using a low-cost magnetron. Owing to their high maintenance costs, most of existing millimeter-wave radars are not suitable for long-term (several months or longer) cloud and precipitation observations, which are necessary for monitoring earth environments. This resulted in the development of the new Ka-band frequency modulated continuous wave (FMCW) Doppler weather radar (KaDR), which achieves high cost performance by using a low-power traveling wave tube used in satellites. This study demonstrates the ability of XDR and KaDR measuring equivalent radar reflectivity factor (Z_e) and Doppler velocity (V_d) accurately.

To assess the accuracy of Z_e and V_d measured by XDR and KaDR, field experiment data collected during 25-26 October 2009 at the Shigaraki MU observatory (34°51'N, 136°06'E) were used. Data of Micro rain radar (MRR) and a 1.3575 GHz Doppler radar named LQ-7 were used to assess the Z_e and V_d measured by XDR and KaDR. Z_e and V_d measured by XDR, KaDR, and LQ-7 were computed from Doppler spectra using the moment method. Figure shows an example of the assessment results. Correlations greater than 0.9, regression slopes close to 1.0, and regression intercepts close to 0.0 indicate that XDR and KaDR measured Z_e and V_d accurately.

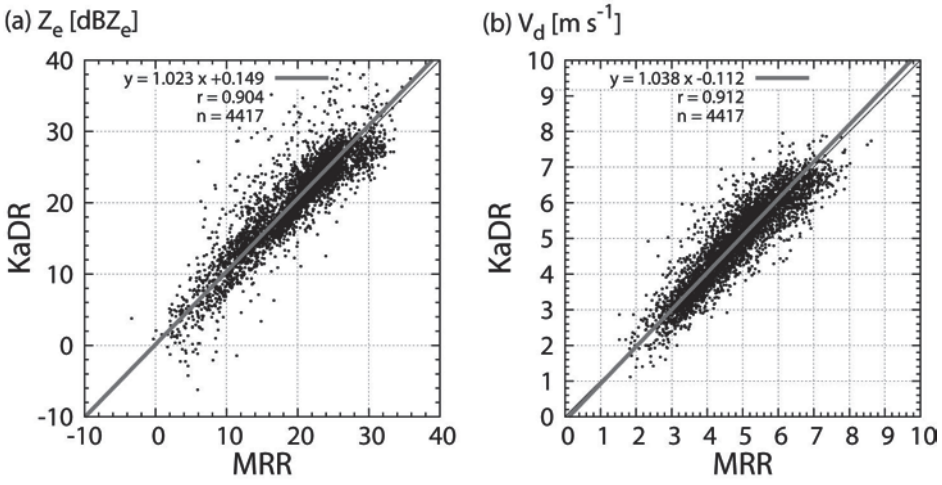

Scatter plot of Z_e (left) and V_d (right) measured by MRR and KaDR.

Acknowledgements

XDR and KaDR were designed by Mitsubishi Electric TOKKI Systems Corporation, and their development were supported by the Meteorological Research Institute (MRI), Japan Meteorological Agency (JMA) under the program of Special Coordination Funds for Promoting Science and Technology named "Japanese Cloud Seeding Experiments for Precipitation Augmentation (JCSEPA)". JCSEPA program is funded by the Ministry of Education, Culture, Sports, Science and Technology of Japan (MEXT).

Development of the digital receiver for wind profiler radar using software defined radio technique

**(Graduate School of Informatics,
Laboratory of Radar Atmospheric Science, RISH, Kyoto University)**

Youhei Wakisaka

It is important to observe atmospheric turbulence in order to clarify developing processes of the atmospheric boundary layer. However, it is not so easy to observe the atmospheric turbulence. In FY2003, the MU radar was equipped with a ultra-multi-channel system, which enabled us to observe three dimensional structures of the atmospheric turbulence by means of radar imaging techniques. Limitation of the MU radar is that it cannot observe the lower part of the atmosphere below 2 km. Therefore we have developed digital receivers which can receive the signal from multiple antennas of the 1.3-GHz wind profiler radar (LQ7) for observing the atmospheric boundary layer (see Figure 1).

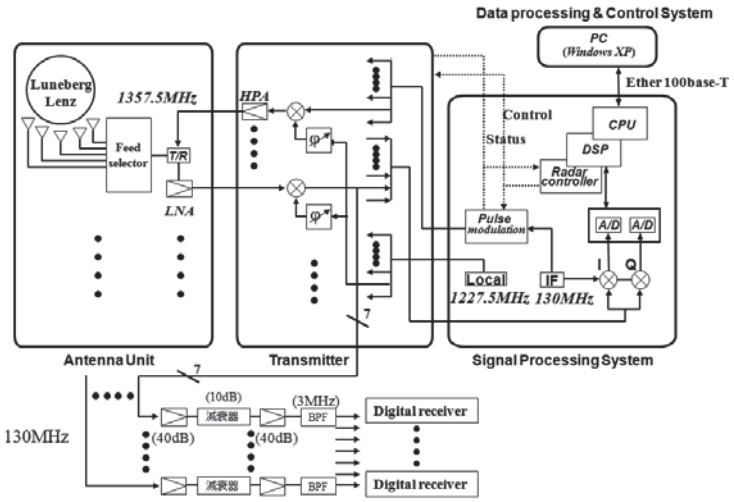

Figure 1. Block diagram of an LQ7 wind profiler radar and developed digital receivers.

The purpose of this study is to develop the digital receivers which can be used in multi-frequency and multi-channel modes. Thereby, range and spatial resolutions will be improved by observations of frequency domain interferometry (FDI) and spaced domain interferometry (SDI). In this study, we used software defined radio receiver, USRP2, for the development of the digital receiver. First, we developed receiver using a GNU Radio software library to control USRP2. We developed techniques to synchronize the receiver with the transmission of LQ7 and for data acquisition. We conducted test observations using a developed receiver and LQ7, and evaluated the capability of the receiver from the observation results of Doppler spectra and velocities. We confirmed that the developed receiver correctly operates and has equal performance with LQ7. However, we found an unavoidable problem regarding the synchronization among plural receivers. In order to solve this problem, we developed a new receiver with Universal Hardware Driver (UHD) which is a driver provided from the manufacturer company of USRP2. The receiver with UHD enables us to synchronize several receivers by using GPS clock. We developed techniques to synchronize the receiver with the transmission of LQ7 and for data acquisition, and conducted the test observations. As shown in Figure 2, we confirmed that the developed receiver correctly operated.

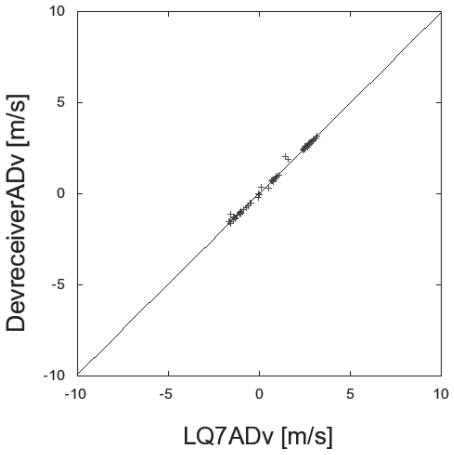

Figure 2. Scatter plot of radial Doppler velocities obtained by LQ7 itself (horizontal axis) and the developed digital receiver (vertical axis).

Development of Particleboard using Citric Acid and Sucrose.

**(Graduate School of Agriculture,
Laboratory of Sustainable materials, RISH, Kyoto University)**

Osamu Sugihara

Introduction

In the wood industry, various kinds of synthetic resins derived from fossil resources are used as binders. However these resources are not renewable and are being steadily exhausted. Therefore, the alternative adhesives derived from non-fossil resources are required. In this study, new natural adhesive composed of citric acid and sucrose was used as an adhesive for particleboard, and physical properties were examined.

Materials and Methods

Recycled chips with the moisture content (MC) of 4-8 %, citric acid and sucrose were used in this experiment. A certain weight ratio of citric acid and sucrose was dissolved in water, and the solution was used as an adhesive. The weight ratios of citric acid and sucrose were adjusted to 100:0, 75:25, 50:50, 25:75, 0:100. The adhesive was sprayed onto recycled chips in a weight ratio of 5 to 40 wt%, and then MC of chips were conditioned by air drying or oven drying at 40 °C. After forming a mat, the mat was hot-pressed. The pressing temperature and time were adjusted to 140 to 240 °C, 10 minutes, respectively. For comparison, the particleboards using an isocyanate resin were manufactured in the same condition (adhesive content=8 wt%, temperature=200 °C). The bending test, internal bond test, and water resistance test based on JIS A 5908 were performed to evaluate the physical and mechanical properties of particleboards.

Results and discussion

Fig. 1 shows the bending properties of particleboards. Mechanical properties were improved with the increase of pressing temperature up tp 200 °C, and the modulus of rupture (MOR) and the modulus of elasticity (MOE) pressed at 200 °C achieved 22 MPa, and 4.8 GPa, respectively. This value of MOR and MOE exceeded the standard level of JIS 18type, and the value of MOE was higher than that of the board bonded with the isocyanate resin. The water resistance was also similar to that using the isocyanate resin.

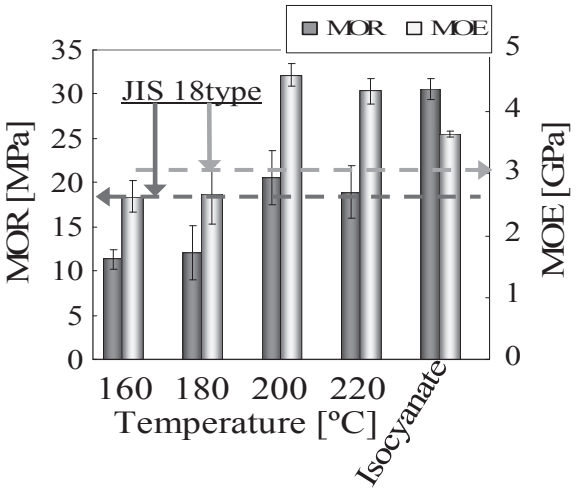

Fig1. Effects of the pressing temperature on bending properties
The weight ratio of citric acid and sucrose is 25:75.
Adhesive content is 20 wt%.

Characterization of NO_2 sorption by Japanese cedar wood

**(Graduate School of Agriculture,
Laboratory of Sustainable materials, RISH, Kyoto University)**

Mimei Nishioka

Introduction

In recent years wood has been found to sorb air pollutants such as NO_2. Japanese cedar wood showed especially high NO_2 sorption ability compared with other wood species. The morphological structure, the components and the moisture of wood were the factors affecting the sorption of pollutants. However, influences of these factors are not evaluated systematically and comprehensively so far. This research discusses the characterization of the NO_2 sorption phenomenon of Japanese cedar wood.

Materials and Methods

Materials; 40 year-old natural dried heartwood of Japanese cedar (*Cryptomeria japonica* D.DON) from Osaka was used. In order to investigate the effect of tracheid structure and grain size, disk-shaped end grain sample (d: 10mm(R), t: 1.5mm(L)), and 3 sizes of wood flour were prepared respectively. To investigate functions of wood components, extracted wood flour, holocellulose and α-cellulose were prepared. To investigate the effect of moisture, humidified (MC: 0-12%) wood flour and components were prepared.

Methods; In an incubator at 20˚C, samples set into U-shaped glass tube or Teflon tube were aerated with concentrated NO_2 (1000ppb, flow velocity: 560ml/min). NO_2 and NO concentration before and after passing through the samples were monitored with a NOx analyzer. NO_2 sorption ratio and NO generation ratio were calculated and compared among various samples. The relative humidity of the aeration gas was controlled to be same with the humidified samples.

Results and discussion

Fig.1 shows the NO_2 sorption ratio of wood components in dry and humidified condition. The moisture content affected the NO_2 sorption ratio for each component. NO_2 sorption ratio of humidified samples became larger than dried samples except in case of hemicelluloses. It seemed that lignin and extractives gave larger effect on the sorption phenomenon in humidified condition.

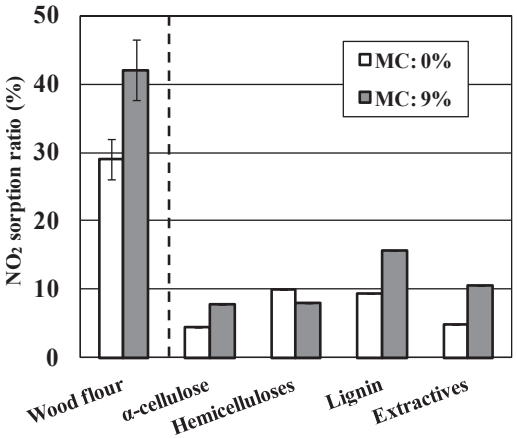

Fig1. NO_2 sorption ratio of dry and humidified samples

NO_2 : 1000ppb Flow velocity : 560ml/min
T : 20℃ RH : 0, 56 ±5%
Sample weight : 0.5g (Wood flour)
Component ratio : α-cellulose 41.8%
Hemicelluloses 24.0%
Lignin 31.6%
Extractives 2.6%

Thrust Analysis of Magnetic Sail Spacecraft with a Superconducting Coil

**(Graduate School of Engineering,
Laboratory of Space Systems and Astronautics, RISH, Kyoto University)**

Yuri Mukai

Recently, a new space propulsion system called magnetic sail has been studied for possible application to deep space missions and interplanetary missions. An artificial magnetic field is expanded around a spacecraft by mounting a superconducting coil onboard. The spacecraft magnetic field interacts with the solar wind, which is a plasma flow from the sun, and generates a thrust force to the spacecraft. The magnetic sail produces thrust by imparting momentum flux of the solar wind to the spacecraft, requiring no propellant. This thesis aims at revealing the thrust mechanism of the magnetic sail considering the characteristics of the type II superconductors.

We investigate the interaction between the superconducting coil and the magnetic field by computer simulations and experiments. In the computer simulations, we analyze the magnetic field distribution in the superconducting coil in the condition of the presence of an external magnetic field assuming the Bean model. The external magnetic field is produced by the induced electricity at the boundary region of the magnetosphere around the spacecraft, as a result of interaction between the spacecraft induced magnetic field and the solar wind. The results show a good agreement between the thrust force of the magnetic sail with a superconducting coil and that of an ideal current loop. The current density in the superconductor coil is large. Thus the Lorentz force to drive the thrust becomes large, although the quantized magnetic fluxes penetrating into the coil are very few.

To confirm this result by experiments, we designed a thrust measurement system of the magnetic sail. We made a small superconducting coil and sustained it in a chamber. As a result, the thrust force of the coil becomes 0.19 N when the current in the coil is 80 A in the exterior magnetic field. The thrust in the simulation is 0.20 N. These results indicate that the thrust with the coil is the same as that with an ideal current loop.

References

[1] Mukai, Y., Funaki, I., Nakamura, T., Kojima, H., Koyama, T., and Yamakawa, H. “Ground Thrust Measurement System for Superconducting Magnetic Sail Spacecraft,” Paper IAC-10.C4.8.4., 61st International Astronautical Congress, Prague, Czech Republic, September 26-October 1, 2010.

[2] Mukai, Y., Funaki, I., Nakamura, T., Kojima, H., and Yamakawa, H.,”Thrust Analysis of Magnetic Sail Using a Superconducting Coil,” JSASS Paper 1P14, Proceeding of the 54th Symposium on Space Science and Technology, November 17-19, 2009, Shizuoka (in Japanese).

Spacecraft Relative Dynamics and Control Using Geomagnetic Lorentz Force

**(Graduate School of Engineering,
Laboratory of Space Systems and Astronautics, RISH, Kyoto University)**

Shu Tsujii

In this thesis, we investigated dynamics and control aspects of a charged satellite using the Lorentz force. The concept of the Lorentz-augmented charged satellite realizes propellant-less electromagnetic propulsion, using the interaction between an electro-statically charged satellite and the Earth's magnetic field. Charging of satellites can be controlled by devices like ion or electron gun. The devices are smaller and lighter than conventional chemical thrusters and suitable to be carried by small-size satellites.

We investigated relative dynamics of two satellites orbiting around the Earth. One is a non-charged satellite called a target satellite, and the other is a charged satellite located near the target satellite on a circular orbit. We study the effect of the Lorentz force on the relative motion of the chaser satellite with respect to the target satellite on an elliptic orbit or on a circular orbit as a special case. We consider the general elliptic reference orbit for the target satellite using a tilted dipole Earth magnetic field. We derive the equations of the relative motion based on the Tschauner-Hempel equations. The circular orbit case can be given by substituting the condition of the circular orbit based on the Clohessy-Wiltshire equations.

Next, we investigated the conditions for transfer between two arbitrary positions using linearized equations when the target satellite lies in the plane of the Earth equator as a reference case. We derived the relation between the periodic orbit conditions of the chaser satellite. The condition for realizing transfer trajectory of the chaser satellites was also provided. Moreover, it was found that, if the inclination of the target satellite orbit is non-zero, the chaser satellite is able to move between any two positions on the target satellite's orbital plane.

Finally, by introducing a non-linear optimization method, called sequential quadratic programming method, we examined the possibility to control the chaser satellite position, when the target satellite orbit has non-zero inclination in the tilted dipole magnetic field moving on an elliptical Earth orbit, and various orbits were successfully proposed by controlling the charge of the chaser satellite.

References

[1] Tsujii, S., Yamakawa, H., Yano, K., and Bando, M., “A Note on the Satellite Formation Flight Using Lorentz Force,” Paper JSASS-2009-4480, Proceeding of the 53rd Symposium on Space Science and Technology, September 9-11, 2009, Kyoto (in Japanese).

[2] Tsujii, S., Yano, K., Bando, M., and Yamakawa, H., “Dynamics and Control of Lorentz Augmented Satellite Formation Flight,” Paper JSASS 1I05, Proceeding of the 54th Symposium on Space Science and Technology, November 17-19, 2010, Shizuoka (in Japanese).

Study on High Temperature Superconducting Coil System for Magnetic Sail Spacecraft

**(Graduate School of Engineering,
Laboratory of Space Systems and Astronautics, RISH, Kyoto University)**

Tomokazu Koyama

Magnetic sail propulsion system has been studied for exploring deep space because of an efficient and high thrust. Thrust is subjected to the interaction between solar wind momentums and the artificial magnetic field of an excited superconducting coil installed in the spacecraft. To obtain large thrust efficiently, the superconducting coil is indispensable for magnetic sail. Therefore, we investigate the superconducting coil system for the magnetic sail spacecraft.

Superconductors have nonlinear conducting characteristics. Especially, we need to estimate the critical current of the superconducting coil. We obtain the basic conducting characteristics from experiments using short length superconductor of Bi2223 and YBCO. Experimental results provide percolation transition models that express the conducting feature. We calculate the conducting characteristics of the large size coil for magnetic sail with the percolation transition models.

A large current runs into the superconducting coil cooled down by conduction cooling in the magnetic sail. Therefore, thermal design of the coil considering heat generation in the coil and cooling capacity of the cooler is very important. We obtain the thermal diffusivity of Bi2223 and YBCO from experiments and thermal analyses. Calculating 2D heat equation of the coil with the thermal diffusivity, we investigate the thermal stability of the coil.

Generally, a conventional power supply for a superconducting coil has very heavy weight. There is no high current power supply suitable to be installed in spacecraft. We examine lightweight and high current power supply systems for the magnetic sail. Then, we propose the DC/DC converter power supply system for the magnetic sail. Since the DC/DC converter has voltage ripples of which influence on the superconducting coil is not understood, we investigate the influence experimentally.

References

[1] Koyama, T., Funaki, I., Nakamura, T., Kojima, H., and Yamakawa, H. “Thrust Control System for Magnetic Sail Spacecraft under Variable Solar Wind Environment,” Paper IAC-10.C4.8.6, 61st International Astronautical Congress, Prague, Czech Republic, September 26-October 1, 2010.

[2] Koyama, T., Funaki, I., Nakamura, T., Kojima, H., and Yamakawa, H., ”Power Subsystem for Superconducting Coil Control of Magnetic Sail”, JSASS Paper 1B01, Proceeding of the 54th Symposium on Space Science and Technology, November 17-19, 2009, Shizuoka (in Japanese).